Cross Correlation Analysis of Ionospheric Parameters with Symmetric-H and Auroral Electrojet Indices during Geomagnetic Storms

Samyam Pudasaini[1], Binod Adhikari[2], Rohit Bhattarai[1], Iva Kumari Lamichhane[1], Manghang Limbu[1], Pramod Kamal Kharel[1], Aasis Bhandari[1], Pitri Bhakta Adhikari[1]

[1]Department of Physics, Tri-Chandra Multiple College, Tribhuvan University, Kathmandu, Nepal
[2]Department of Physics, St. Xavier's College, Maitighar, Kathmandu, Nepal

Key Points:

- There is a strong evidence of pre-storm phenomenon occurring at least a few hours and more than 24 hours prior to the main phase of the geomagnetic storms.
- The TEC and foF2 parameters have strong dependence with latitudes for the events with Sudden Storm Commencement (SSC) in the middle latitudes region.
- The highest correlations of geomagnetic indices with ionospheric parameters are mostly observed one day prior to main phase of geomagnetic storm.

Corresponding author: Priti Bhakta Adhikari, pbadhikari09@gmail.com

Abstract

This paper investigates the effects of geomagnetic storms of 25-27 September 2011, 16-18 March 2013, and 6-8 September 2015 over five mid latitudes stations (Dourbes, Fairford, Moscow, Rome, and Roquetes) and performs a cross correlation analysis of ionospheric and solar parameters during these storms. We observed the highest fluctuations in ionospheric variables during the main phase of storms. In addition, there is strong evidence of pre-storm phenomenon occurring at least a few hours and more than 24 hours prior to the main phase of the geomagnetic storms. We found that the TEC and foF2 parameters have strong dependence with latitudes for the events with Sudden Storm Commencement(SSC) in mid lattitude region. Relatively low TEC and foF2 can be observed in Moscow which is at the highest latitude among the five stations because of a decrease in the n(O)/n(N2) ratio through out the storm event. However, for the event with gradual storm commencement, there is no evidence of such dependence. The good correlation of Symmetric-H and Auroral Electrojet Indices with ionospheric parameters indicates that the coupling mechanism between magnetosphere and ionosphere produces intense electric field disturbances in the middle low latitudes.

1 Introduction

Geomagnetic storms are produced when the interplanetary magnetic field (IMF) Bz component turns southward, strengthens (IMF Bz < -10 nT), and remains southward for a substantial length of time (longer than ~ 3 hr; (W. D. Gonzalez & Tsurutani, 1987); (W. Gonzalez et al., 1994)). As this happens, a rapid increase of magnetic reconnection processes occurs at the magneto-pause. When IMF-Bz is strongly negative, open field lines are produced by magnetic reconnection between the IMF and the geomagnetic field which allow the passage of mass, energy and momentum from the solar wind to the Earth's magnetosphere. This results in more solar wind energy input into all regions of the earth-atmosphere system, resulting in a geomagnetic storm. Geomagnetic storms are an important space weather phenomenon that, apart from affecting ground and satellite-based technological and high-frequency communications systems, can severely affect the dynamics and structure of the Earth's entire thermosphere and ionosphere. The ionospheric response to a geomagnetic storm is called an ionospheric storm that describes the ionospheric variations due to geomagnetic disturbances.

Geomagnetic activity observed at the Earth is generally attributed to the occurrence of Coronal Mass Ejection (CME) on the Sun and the associated interplanetary shock waves or corotating interaction regions (CIR) produced by high-speed solar wind streams in the interplanetary medium ((Gosling, 1993a); (Gosling, 1993b); (Bothmer & Schwenn, 1994); (Luhmann, 1997); (Crooker & McAllister, 1997)). CMEs are expulsions of mass from the Sun and are generally associated with solar flares or prominences. Once launched from the Sun, CMEs travel through the interplanetary medium and, if directed toward the Earth, reach the Earth in 1–4 days depending on their speed. Therefore in order to predict geoeffectiveness of CMEs, one needs to examine the solar data from near the surface of the Sun and follow them through to the Earth. This is faciliatated by an examination of ground-based and space-based multi-instrument data sets.

Ionosphere is the layer of the atmosphere that lies between 60 km and 1000 km above the Earth surface and has a great importance in high frequency (HF) and satellite communications because of its electrical and ionic structure. The ionization characteristics and electron density distribution vary according to the location on Earth, time, solar, geomagnetic and seismic effects. Ionosphere consists of three distinct layers, namely D, E, and F. The F layer is the most significant layer in the ionosphere and the central part has the greatest electron density. During day time the F layer splits into F1 and F2 layers. F2-layer, having the highest electron density, is the most stable layer for HF communications and it has major importance in satellite communications ((Kolawole, 2003)).

The F2 region is considered the most difficult and anomalous ionospheric region to predict (Hargreaves, 1992). In order to model this region, several authors have used the F2 critical frequency (foF2) and the F2 region peak height (hmF2) parameters. These parameters depend on various geophysical parameters including local time, season, solar and geomagnetic activity conditions and are believed to describe the overall behavior of the F2 layer ((Sethi & Pandey, 2001); (Richards, 2001); (Kawamura et al., 2002); (J. Liu et al., 2003); (Lei et al., 2005); (L. Liu et al., 2006); (S.-R. Zhang & Holt, 2008); (Moen et al., 2008); (M.-L. Zhang et al., 2009); (Souza et al., 2010), and references therein). A better understanding of the variability and modeling of foF2 and hmF2 parameters is crucial for the development of ionospheric prediction capabilities, improvements in existing ionospheric models, and for radio propagation studies.

Studies have shown that, there are strong disturbances induced in the F-region of the ionosphere during strong geomagnetic storms. These perturbations cause large enhancements and reduction of electron density at the F2 region described as positive and negative ionospheric storm effects respectively.(see, e.g., (Fuller-Rowell et al., 1994); (Volland, 1995); (Buonsanto, 1999); (Mendillo, 2006).) The occurrence of positive and negative storm effects depends upon the latitude, local time, and phase of the storm ((Fuller-Rowell et al., 1994)).

The ionospheric variations can be determined from the total electron content (TEC) or from the critical frequency of the F2-layer (foF2), which is a direct measure of the peak electron density (NmF2) of the F2-region ionosphere. The positive ionospheric storms have a high density of electrons and negative storms contain a lower density ((Fagundes et al., 2016)). The total electron content (TEC) is used to measure these densities, and is a key variable used in data to record and compare the intensities of ionospheric storms.

Ground magnetometer measures the integrated effect of all these disturbed time and also quiet time ionospheric and magnetospheric currents. Geomagnetic indices like Disturbance storm time index (Dst) and Symmetric H-component (SYM/H) index mainly represent ring current intensity during geomagnetic storms ((Sugiura et al., 1964); (Rangarajan, 1989); (Wanliss & Showalter, 2006)), derived using the longitudinally distributed chain of low latitude ground-based magnetometers. SYM/H is the same as Dst, but it has a 1-minute temporal resolution, which is very useful to study short temporal variations during the geomagnetic disturbances. SYM/H is derived by first subtracting the main geomagnetic field due to internal geodynamo and external Sq induced geomagnetic field variations and then averaging residual fields. Therefore, it is a good proxy for the longitudinally symmetric component of the ring current. SYM/H is an indication of storm ring current intensity and AE gives auroral substorm ionospheric current intensities.

In the present study we investigate the solar and interplanetary conditions that were specific to intense geomagnetic storms of 25-27 September 2011, 16-18 March 2013, and 6-8 September 2015 (minimum SYM/H < -130 nT) in order to understand the relationships between the solar indices and ionospheric parameters associated with intense geomagnetic storms.

2 Data Sources

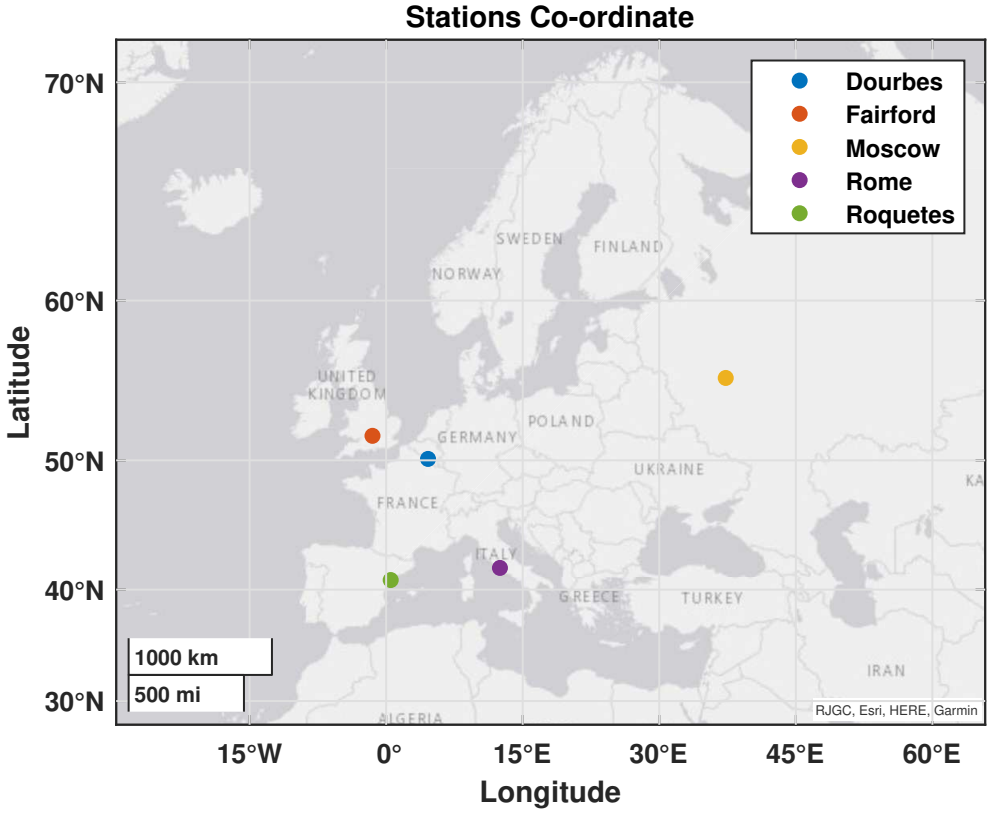

Figure 1. Map of the Stations.

Table 1. Table of stations.

S.No	Stations Name	URSI	Latitude	Longitude
1.	DOURBES	DB049	50.10	4.60
2.	FAIRFORD	FF051	51.70	358.50
3.	MOSCOW	MO155	55.47	37.30
4.	ROME	RO041	41.80	12.50
5.	ROQUETES	EB040	40.80	0.50

Figure 1 shows the map of the ionospheric stations used in this study. The observed F2-layer parameters (foF2, hmF2, and TEC) in this study are obtained from a chain of ionosondes located at Dourbes (50.1° N, 4.6° E, data temporal resolution 5 min), Fairford (51.7° N, 358.5° E, 15 min), Moscow (55.47° N, 37.3° E, 15 min), Rome (41.9° N, 12.5° E, 15 min), and Roquetes (40.8° N, 0.5° E, 5 min) during the geomagnetic storms on 25-27 September, 2011; 16-18 March, 2013; and 6-8 September, 2013. In order to investigate the F2-layer behaviors during low solar activity, the data under geomagnetic quiet-conditions on 17-19 March, 2017 are selected. The data are available at the Digital Ionogram Data Base (DIDBase) (`https://giro.uml.edu/didbase/`).

The modulation of solar wind (SW) and interplanetary magnetic field (IMF) components (Bx, By, and Bz) high-resolution (1 min) data were obtained from OMNI Database (`https://omniweb.gsfc.nasa.gov/form/omni_min.html`).

The sudden storm commencement (SSC) is often served as a reference time for the onset of a magnetic storm. The reliability of SSC for the storm onset has been argued for a long time. As a result, some investigators choose the main phase onset of the storm instead of SSC as the start time of a storm [e.g., (Prölss, 1995). Here we use SSC to indicate the onset of a magnetic storm for storms with a sudden commencement, except for the event on 06-08 September, 2015 because it only had a gradual commencement. The SYM/H index is used to indicate the evolution and intensity of geomagnetic storms.

3 Result

3.1 Event-1: 25-27 September, 2011

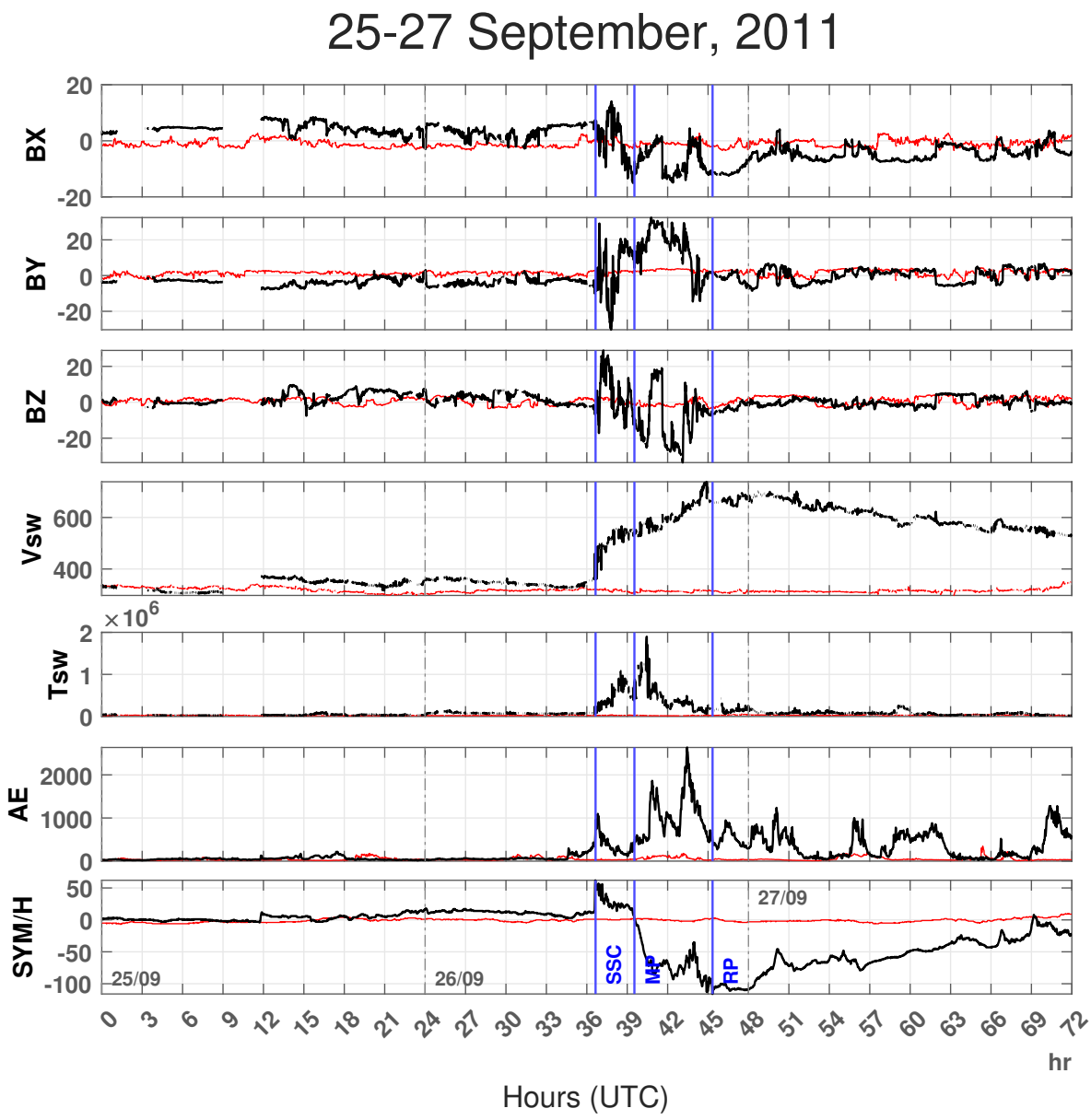

Figure 2. Variation in components of the magnetic field (in GSM co-ordinates), Bx (nT), By (nT) and Bz (nT), solar wind velocity Vsw (km/s), plasma temperature Tsw (K), geomagnetic indices, SYM/H (nT), and AE-index (nT) during Super Sub-Storm of 25–27 September, 2011. The red curve denotes the variation during quiet days (18-20 March, 2017).

Almost halfway through the ascending phase of the 24^{th} solar cycle, a G2 level, moderately strong geomagnetic storm with Kp index of 6 occurred on 26 September, 2011 due to a concentrated blast of electrically-conducting solar wind plasma and tangled magnetic field lines from region 1302 (N12E47) of the Sun. The region produced a X1.9 flare,

a M7.1 long duration x-ray flare and a M5.8 x-ray flare on 24 September (Source: `https://www.spaceweatherlive.com/`). Figure 2 displays temporal evolution of interplanetary parameters Bx, By, Bz, solar wind velocity (Vsw), solar wind temperature (Tsw), geomagnetic activity indices AE (Auroral Electrojet) index, and SYM/H index for 25–27 September, 2011. The differences between the various parameters during the event (indicated by black curves) and quiet days (indicated by red curves) are observed from the figure 2.

At 12:38 (UTC) of 26 September the sudden storm commencement (SSC) is seen to have occurred when the symmetric horizontal component of the geomagnetic field SYM/H rose sharply from 15 nt to the highest point of 62 nt, indicating the beginning of the initial phase. During this period, all the ionospheric parameters significantly fluctuate while the north-south interplanetary magnetic field Bz altered between positive and negative values a few times with positive (negative) value indicating northward (southward) magnetic field, reaching its minimum of -33.61 nt at 19:07 (UTC) indicating a strong southward magnetic field. It can be observed from Figure 2, minimas in the Bz curve correlate well with maximas in the Auroral Electrojet (AE) index. At 19:27 (UTC), 20 minutes after Bz reached its minimum, AE-index reached its peak intensity of 2636 nT which corresponds well with the results of (Marques de Souza et al., 2018). Large amount of energy-momentum is transferred into the Earth's magnetosphere from the solar wind which is indicated by high AE index (Pandit et al., 2021). This spike in AE index can be attributed to high southward interplanetary magnetic field (Bz) as the field components parallel to the ecliptic have no significant effect on sub storms (Foster et al., 1971). IMF-Bz getting negative also causes the electric field linking magnetosphere-ionosphere to increase (Adhikari et al., 2018). Correlation between interplanetary magnetic fields Bx and Bz can be also observed in Figure 2 as the plasma flow speed (Vsw) started increasing from the initial phase throughout the main phase as was shown by (Youssef et al., 2012). The plasma velocity (Vsw) reached its peak, 738.6 km/s at 20:53 (UTC), at the end of the main phase and decreased throughout the recovery phase. Around this time, the solar wind temperature (Tsw) had already cooled down reaching its peak 1.89×10^6 K earlier at 16:27 (UTC) around the beginning of the main phase. The recovery phase started when the SYM/H index was recorded to be rising after reaching its lowest at -113 nt at 20:54 (UTC).

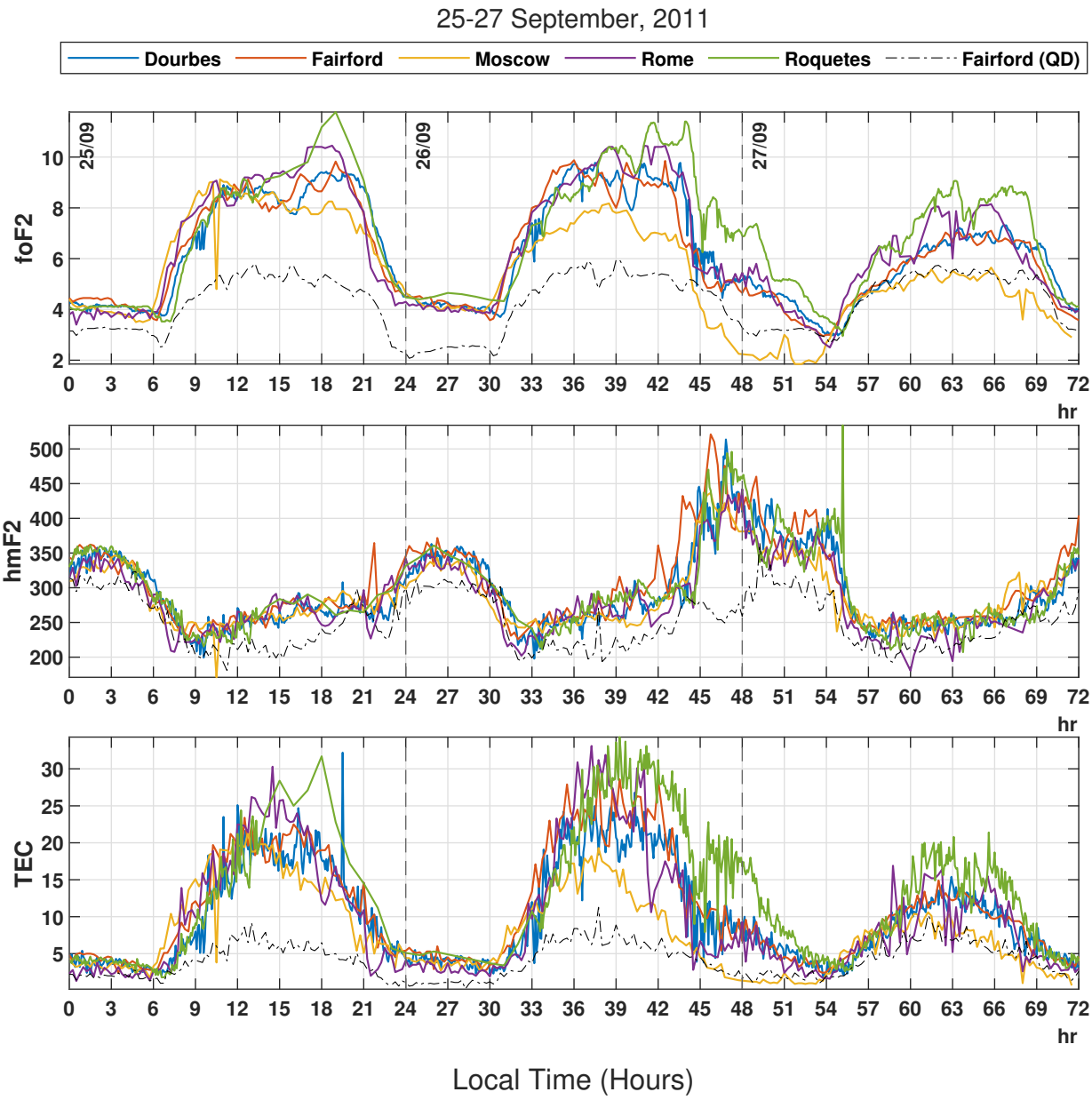

Figure 3. Changes in ionospheric parameters: F2-region critical frequency (foF2) in MHz, Total electron content (TEC) in ($\times 10^{16} m^{-2}$), Maximum Ionization Height (hmF2) in km, recorded at stations Dourbes, Fairford, Moscow, Rome and Roquetes during Super Sub-Storm on 25–27 September, 2011. The black curve denotes the variation during quiet days (18-20 March, 2017).

Figure 3 depicts the variations of three different ionospheric parameters: F2-region critical frequency (foF2), maximum ionization height of F2-region (hmF2), and Total Electron Content (TEC) at five different stations: Dourbes, Fairford, Moscow, Rome and Roquetes. All the stations have similar variations because they all lie in the mid-latitude region. The daily variations of day and night cycle can be easily noticed in all five stations. As the sun rises at around 06:30 local time, a sudden rise in foF2 and TEC is noticed in all the stations whereas around this time hmF2 is observed to have almost reached its lowest values around 09:00 (local time) indicating a negative correlation between them.

Relatively low TEC and foF2 can be observed in Moscow which is at the highest latitude among the five stations because of a decrease in the $n(O)/n(N_2)$ ratio throughout the storm event (Klimenko et al., 2017). TEC and foF2 graph in Figure 3 clearly shows latitudinal dependence with high latitude stations having comparatively more negative values and lower latitude stations having more positive values as shown by (W. Liu et al., 2017) and (GAO et al., 2008). Due to this reason, the ionosonde stations at Rome and Roquetes, being at the lowest latitudes, record the highest values of foF2 and TEC.

In panel 1, the average of highest critical frequency during daytime of the 1st day is about 10 MHz which is ~ 5 units ($\sim 100\%$) higher than that of the quiet day. The mean highest TEC on the 1st day is $\sim 25 \times 10^{16} m^{-2}$, which is ~ 17 units ($\sim 200\%$) higher than that of the quiet day (panel 3). This indicates that the positive storm had already started 1 day prior to the event day. Large amounts of energy getting deposited into the thermosphere and leading to a strong enough storm-induced circulation that further increases plasma vertical drift, increasing the electron concentration is the most frequent cause of positive storms but the occurrence of positive storm before SSC is one of the unsolved problems in ionospheric research (Danilov, 2001). During the nighttime of the first day, the lowest critical frequency is ~ 4 MHz which is ~ 2 units ($\sim 100\%$) higher than that of the quiet day and the lowest TEC is $\sim 3{\times}10^{16} m^{-2}$, which is much higher than that of the quiet day. The highest foF2 and TEC on the 2nd day, similar to 1st day, was ~ 5 units (100%) and ~ 20 units($\sim 200\%$) higher than that of the quiet day respectively. Hence the storm remained positive throughout the 1st day (25 September) and throughout the main phase on the 2nd day(26 September). This result matched with (W. Liu et al., 2017) who showed that in middle latitudes, the positive storm prevails during the main phase and decreases during the recovery phase. When the recovery phase started at 21:00 (local time) of the 2nd day (event day), the positive storm started decreasing and remained quiet throughout the 3rd day.

In panel 2, on the 1st day (25 September), the maximum ionization height (hmF2) above all stations remains similar to that of the quiet day. On the second day (26 September) during the main phase, an increase in hmF2 is observed to be ~ 50 km more in all stations as compared to the quiet day. The plasma vertical drift getting increased by storm-induced circulation is the cause of uplifting of the F2 layer (Danilov, 2001). A sudden increase in hmF2 from $\sim$ 300 km to $\sim$ 450 km is observed at 21:00 (local time) (beginning of recovery phase) which is ~ 200 km more than that of the quiet day. Continuous substorm activity building up a high pressure zone in the polar region, reducing poleward-directed winds and enhancing equatorward-directed winds might be the cause of this sudden increase in the height of the F2 layer (Prölss & Očko, 2000). The uplifting decreases and almost coincides with the quiet day in the morning hours of the third day (27 September) and remains so throughout the day.

3.2 Event-2: 16-18 March, 2013

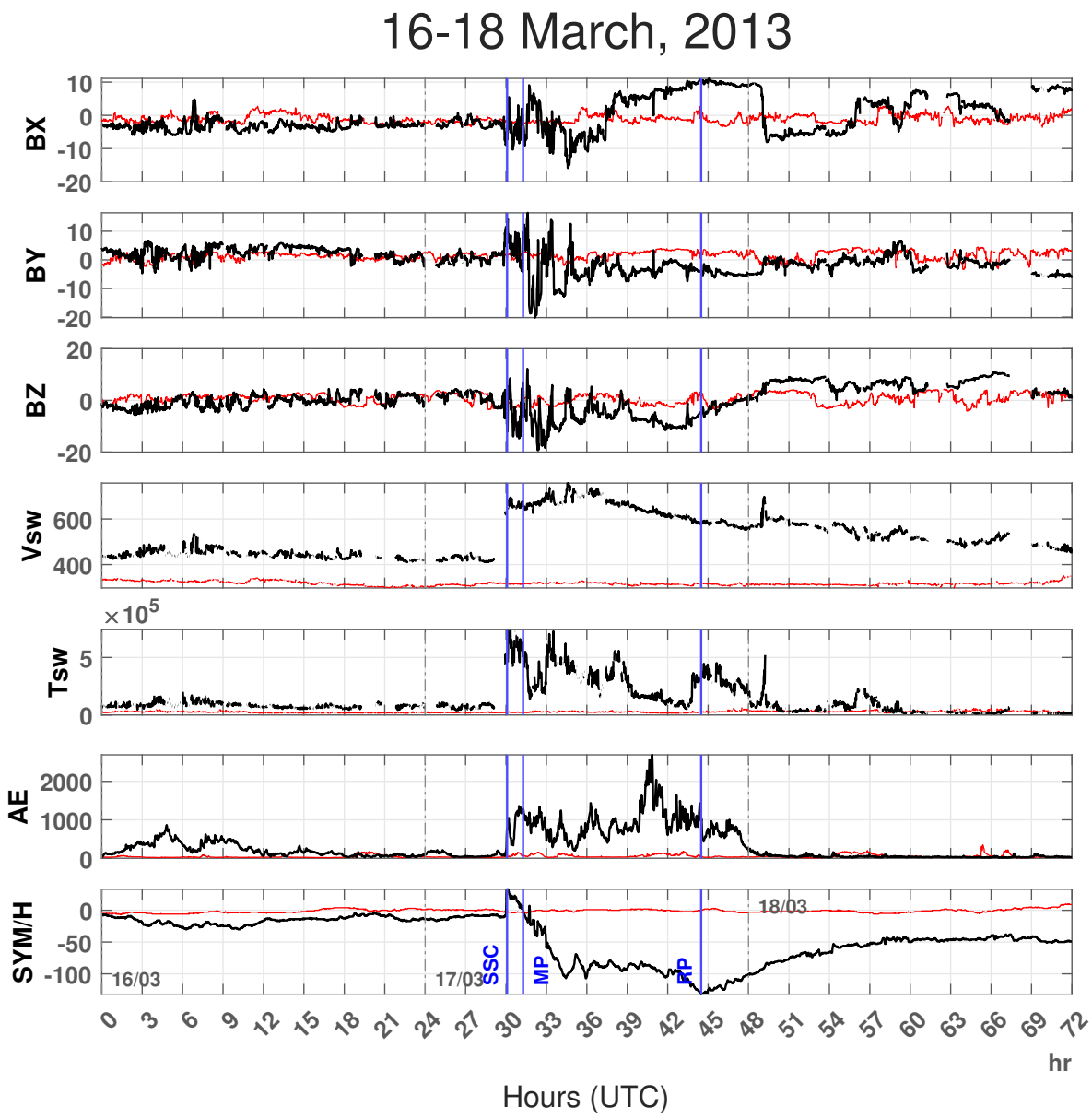

Figure 4. Variation in components of the magnetic field (in GSM coordinates), Bx (nT), By (nT) and Bz (nT), solar wind velocity Vsw (km/s), plasma temperature Tsw (K), geomagnetic indices, SYM/H (nT), and AE-index (nT) during Super Sub-Storm of 16–18 March, 2013. The red curve denotes the variation during quiet days (18-20 March, 2017).

A G3-Class (Kp = 7) Earth-directed Coronal Mass Ejection (CME) event has been observed on 17 March 2013, which is one of the strongest geomagnetic disturbances recorded during the 24^{th} solar cycle with peak intensity of SYM/H $\sim$ -132 nT. Figure 4 displays temporal evolution of interplanetary parameters Bx, By, Bz, solar wind velocity (Vsw), solar wind temperature (Tsw), geomagnetic activity indices AE (Auroral Electrojet) in-

dex, and the symmetric horizontal component of the geomagnetic field (SYM/H) for 17-18 March 2013.

This storm was triggered by an Earth-directed, coronal mass ejection (Baker et al., 2014) associated with M1.1 type solar flare from the sunspot 1692 (N09W03) on 15 March 2013 at 07:00 UT. The incoming CME enhances the Bz (north-south) to strong northward and solar wind speed raised to 600 km/s at around 06:00 UT on 17 March 2013, while magnetic field components also significantly vary. The sudden enhancement of solar wind density and velocity because of CME hitting on magnetosphere triggers the magnetopause current, which enhances our terrestrial magnetic field, which is registered as a sudden storm commencement (SSC) on SYM/H as shown in figure 4. An immediate onset of intense auroral activity is seen in the AE index, reaching a magnitude as high as 2000 nT, indicating the generation of energy source in the high latitude region. The initial phase lasted for approximately one hour and the main phase began around 7:00 UT, as identified by decrease in SYM/H implying the ring current intensification, and SYM/H index reached a first minimum of around -110 nT around 10:00 UT on 17 March. Then it stayed nearly steady until it attained a second minimum of about -132 nT at ∼20:30 UT before recovery which means that the main phase lasted for around 13 hours. The recovery phase lasted for more than 3 days as indicated by an increase in the SYM/H index.

There is a directional discontinuity (DD) at ∼01:12 UT on 18 March (shown by a blue vertical line) clearly observed in the IMF components, solar wind temperature, and solar wind velocity. The IMF Bz turns northward after the directional discontinuity which contributes to a prompt magnetic storm recovery. This northward turning causes a cessation of auroral activity due to reduced magnetic reconnection (Verkhoglyadova et al., 2016). Directional discontinuities in Interplanetary Coronal Mass Ejection is an important factor in determining the geoeffectiveness of the event since they are characterized by sharp changes in coupling functions (Lugaz et al., 2015). A gradual decrease in auroral activity and then a total cessation during the northward IMF interval is observed (Du et al., 2011). The SYM/H index is observed to recover completely after about 3 days. This geomagnetic storm is caused by the double action of southward IMF Bz in the sheath causing the storm onset and southward IMF Bz in the MC intensifying the storm.

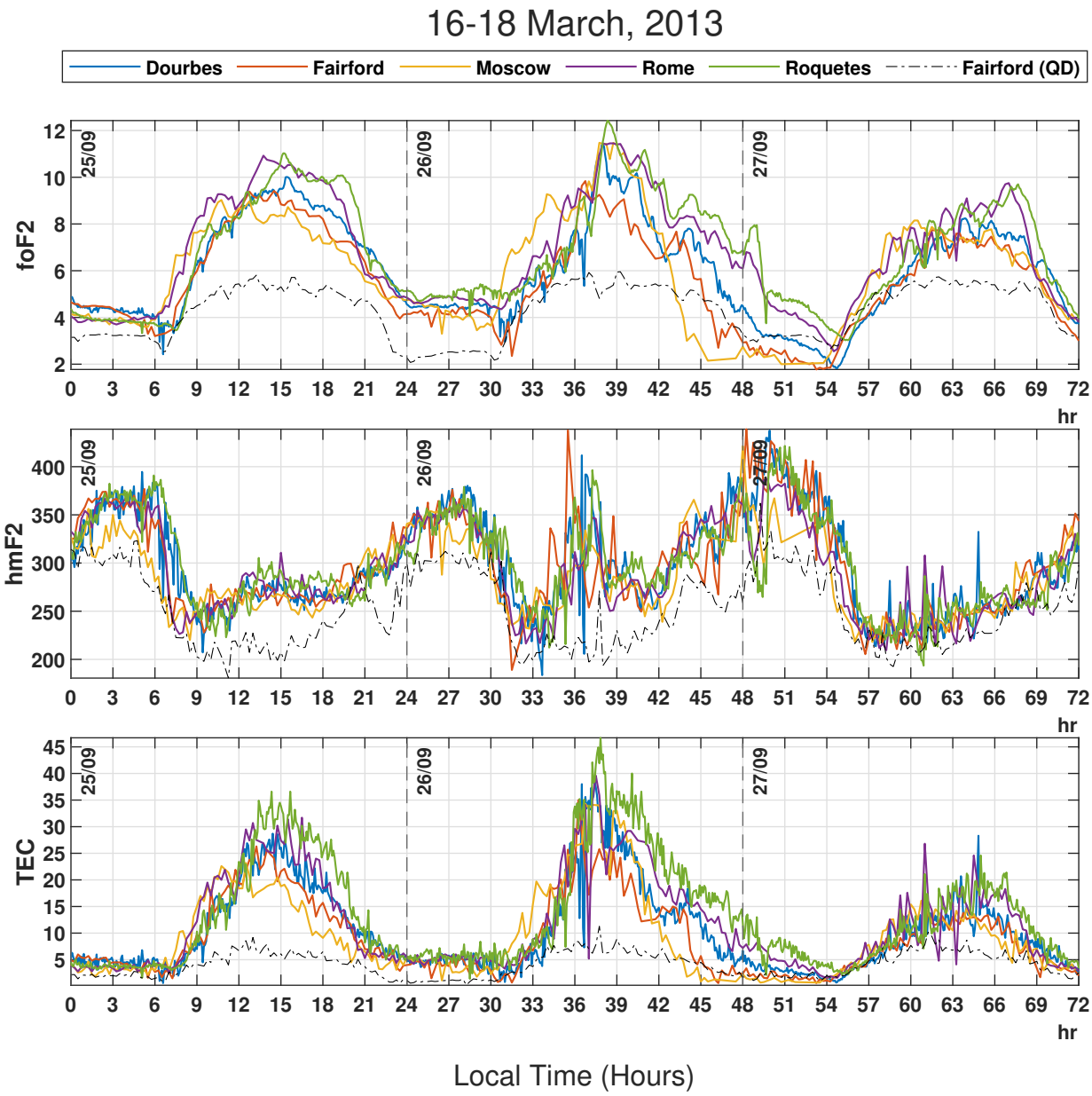

Figure 5. Change in ionospheric parameters, F2-region critical frequency (foF2) in MHz, Total electron content (TEC) in ($\times 10^{16} m^{-2}$), Maximum Ionization Height (hmF2) in km, recorded at stations Dourbes, Fairford, Moscow, Rome and Roquetes during Super Sub-Storm on 16–18 March, 2013. The black curve denotes the variation during quiet days (18-20 March, 2017).

Figure 5 shows F-2 layer parameters (fof2, hmF2, and TEC) between 16-18 March, 2013. The top panel shows the geomagnetic index foF2, the middle panel shows the geomagnetic index hmF2, and the bottom panel shows the geomagnetic index TEC obtained from ionograms of Dourbes, Fairford, Moscow, Rome, and Roquetes.

Similar to event 1, Moscow, being at higher latitude, has the lowest TEC and foF2 among the five stations for reasons similar to mentioned above in event 1 because of a decrease in the $n(O)/n(N_2)$ ratio throughout the storm event (Klimenko et al., 2017). Latitude dependence can be observed in the graph of TEC and foF2 graph as pointed

out in (W. Liu et al., 2017) and (GAO et al., 2008). Similarly, the ionosonde stations at Rome and Roquetes, being at the lowest latitudes, record the highest values of foF2 and TEC.

The average of highest critical frequency during daytime of the 1st day is about 10 MHz in panel 1 which is ~ 5 units ($\sim 100\%$) higher than that of the quiet day. The mean highest TEC on the 1st day is $\sim\ 25 \times 10^{16} m^{-2}$, which is $\sim\ 18$ units($\sim\ 200\%$) higher than that of the quiet day (panel 3). Here, the positive storm had already started 1 day prior to the event day. The lowest critical frequency during the nighttime of the first day is 5 MHz which is 2 units higher than that of the quiet day and the lowest TEC is $\sim 5 \times 10^{16} m^{-2}$, which is much higher than that of the quiet day. The highest foF2 and TEC on the 2nd day, similar to 1st day, was ~ 5 units and ~ 25 units higher than that of the quiet day respectively. This indicates that the storm remained positive throughout the 1st day (16 March) and throughout the main phase on the 2nd day (17 March). The positive storm started decreasing when the recovery phase started at around 20:30 (local time) of the 2nd day (event day) and remained less positive throughout the 3rd day.

On the 1st and 2nd day (16 and 17 March), in panel 2, the maximum ionization height (hmF2) above all stations showed slight increment. On the third day (18 March), hmF2 remained quiet throughout the day. During the main phase, an increase in hmF2 is observed to be ~ 100 km more in all stations as compared to the quiet day. A sudden increase in hmF2 from ~ 250 km to ~ 350 km is observed at 11:00 (local time) which is ~ 100 km more than that of the quiet day. No significant amount of variation in hmF2 is observed at the event day as compared to the previous day of the event.

3.3 Event-3: 6-8 September, 2015

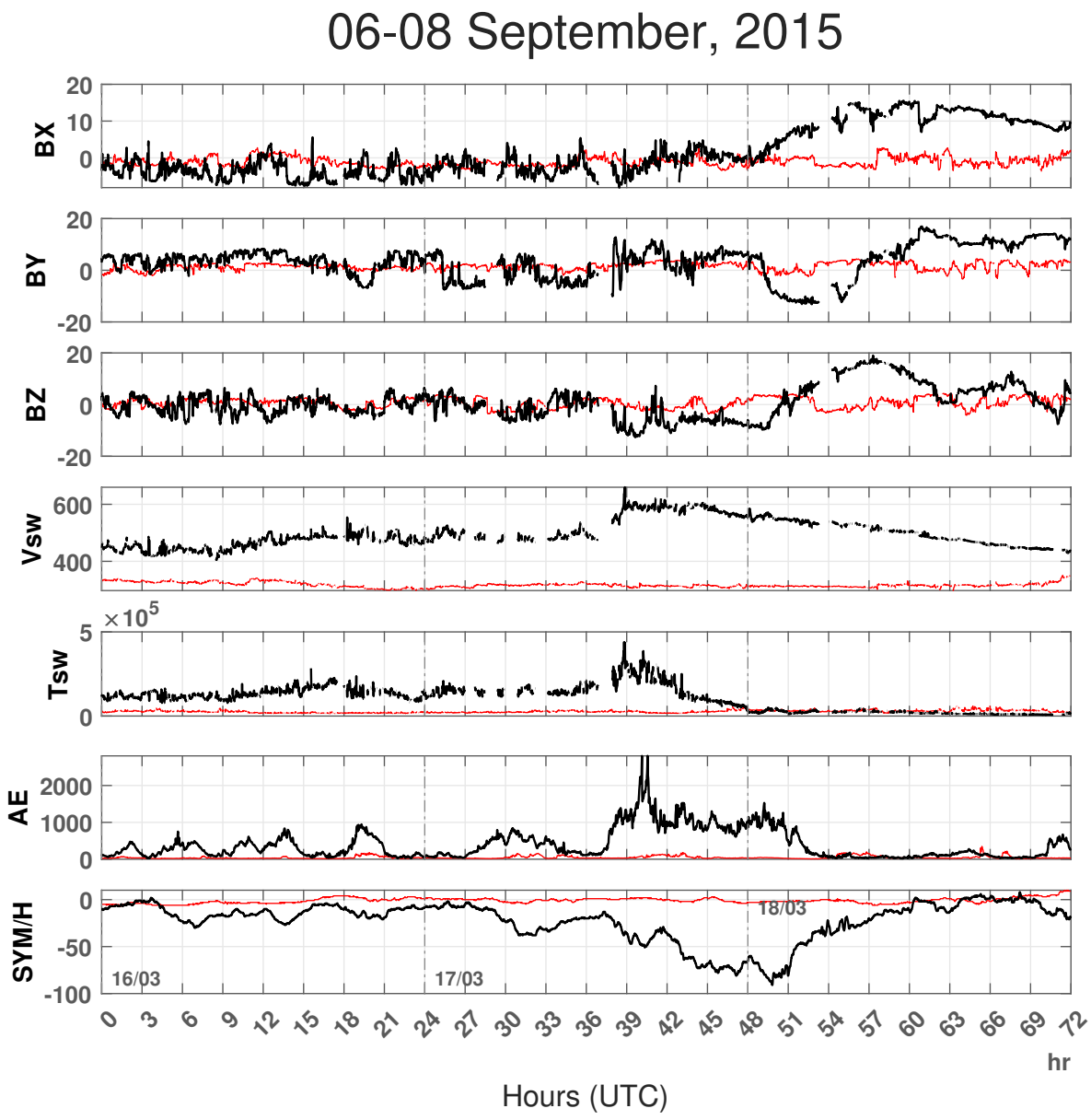

Figure 6. Variation in components of the magnetic field (in GSM coordinates), Bx (nT), By (nT) and Bz (nT), solar wind velocity Vsw (km/s), plasma temperature Tsw (K) , geomagnetic indices, SYM/H (nT) and AE-index (nT) during Super Sub-Storm of 6–8 September, 2015. The red curve denotes the variation during quiet days (18-20 March, 2017).

An unforeseen powerful coronal hole solar wind stream sparked a moderate G2-Class (Kp = 6) geomagnetic storm on 8 September 2015, with peak intensity of SYM/H -83 nT occurring at 02:00 UT on 8 September. Figure 6 shows the temporal evolution of solar wind parameters, the Interplanetary magnetic field components Bx, By, Bz, solar wind velocity (Vsw) , solar wind temperature (Tsw) , AE index and SYM/H, from 6–8 September 2015. It can infer from the graph that there has been a pre-storm phenomena on 06-

07 September with solar wind parameters fluctuating repeatedly on those days. The incoming solar wind has triggered magnetic field components to vary significantly. These values oscillate to either sides of the reference value for Bz and Bz components during the event. However, the Bx component's value oscillates below the reference value till the recovery phase (02:00 UT, 8 September). Similarly, solar wind speed rose to 620 km/s at around 17:00 UT on 07 September. The sudden enhancement of solar wind density and velocity sets off the magnetopause current, represented by SYM/H as shown in figure 7, which amplifies our terrestrial magnetic field citesibeck1990model. An intense auroral activity is seen as the AE index reaches a magnitude as high as around 2800 nT at 16:00 UT on 7 September, indicating the generation of energy sources in the high latitude region. Likewise, Tsw has risen 2 hrs prior to the event which might be due to the pre-storm effect. However, the temperature of solar wind before the storm disturbance is found to be higher than the main phase (MP) of the event, indicating pre-storm phenomena (Adekoya et al., 2012).

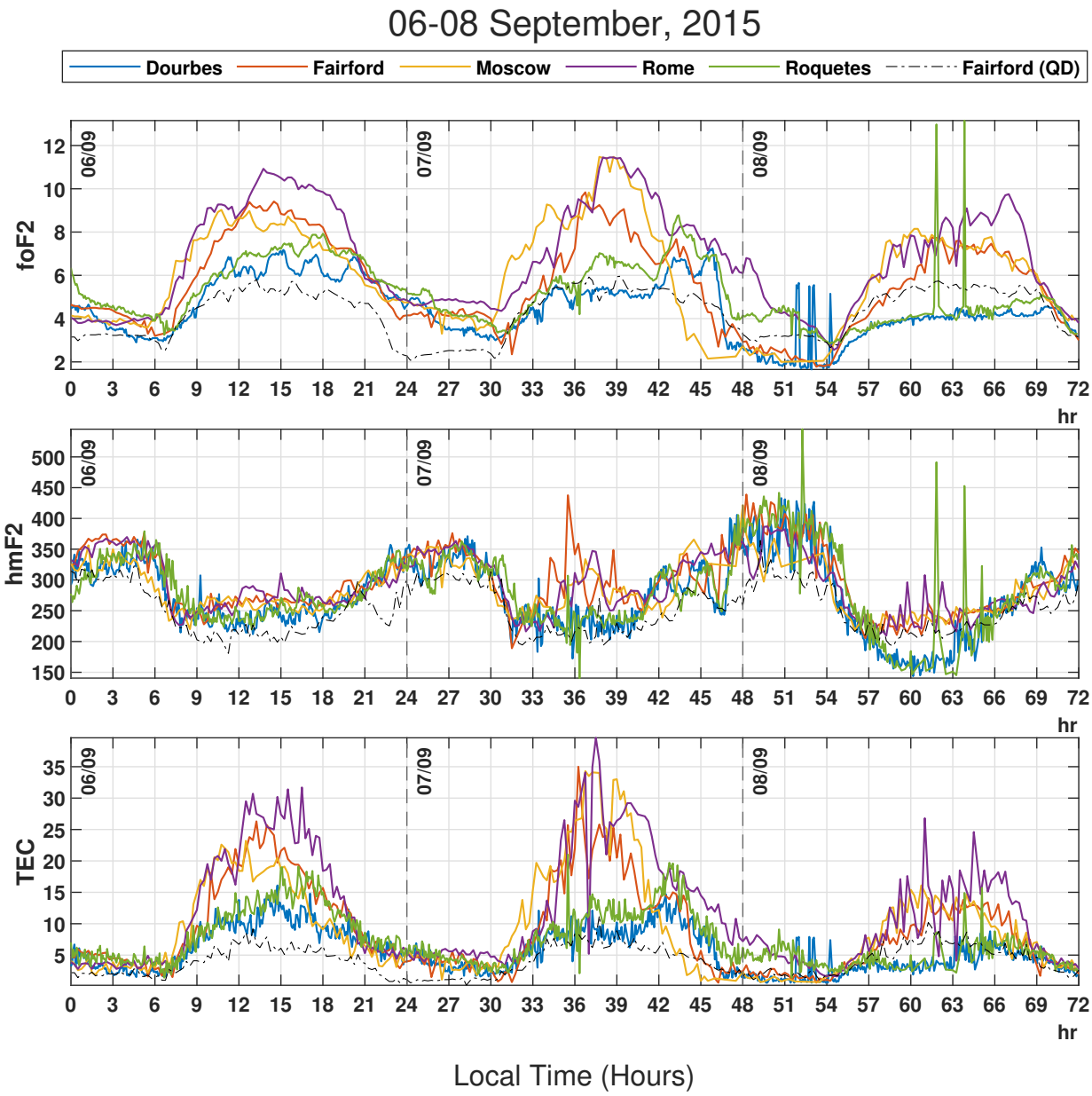

Figure 7. Change in ionospheric parameters, F2-region critical frequency (foF2) in MHz, Total electron content (TEC) in ($\times 10^{16} m^{-2}$), Maximum Ionization Height (hmF2) in Km, recorded at stations Dourbes, Fairford, Moscow, Rome and Roquetes during Super Sub-Storm on 06–08 September, 2015. The black curve denotes the variation during quiet days (18-20 March, 2017).

Values of ionospheric parameters, foF2, hmF2 and TEC, of five different stations due to 2015 geomagnetic storms are plotted in Figure 7. As we have chosen all the stations lying at the mid station, variation of parameters are almost the same for all stations. Value of foF2 increases slightly during the main decreasing phase of SYM/H and decreases during its increasing phase. foF2 in Roquetes has its peak value of 8.7 MHz at 19:25 LT (07 September) about 3.5 MHz more than in quiet days. Around this time, critical frequency is maximum in Rome whereas it has minimum value in Dourbes. The plot of maximum ionization height (hmF2) shows the similar pattern of changes in all

five stations. During the main phase (7th september), maximum increase in hmF2 is observed to be $\sim$ 205 km more in Fairford station as compared to the quiet day. Also, the increase in hmf2 is observed to increase by only 135 KM in Rome and Moscow stations. However, there is only a slight increase in hmf2 in Roquetes and Dourbes stations. The plasma vertical drift getting increased by storm-induced circulation is the cause of uplifting of the F2 layer (Danilov, 2001). The spikes on the graph decrease and almost coincide with the quiet day in the later hours of the third day (08 September).

The TEC plot of five stations shows that the variation pattern is similar to each other. The maximum value of TEC during the main phase is $\sim 40 \times 10^{16} m^{-2}$ about 32 times more than in quiet days, whereas during the recovery phase its value decreases to $\sim 27 \times 10^{16} m^{-2}$. This increase of TEC during the main phase is due to auroral activity, the influx of plasma, and the seasonal effect. TEC content is highest during the equinox seasons (Xiong et al., 2014). Total electron content in Rome attains its maximum, whereas TEC in Dourbes has its lowest value. The TEC and foF2 graph in Figure 7 doesn't show any latitudinal dependence which contradicts the result as shown by (W. Liu et al., 2017) and (GAO et al., 2008).

4 Cross-Correlation Analysis

For all cross-correlation analysis shown in this paper, the y-axis represents normalized correlation coefficients and x-axis represents time lag. Each unit in the x-axis is equivalent to time lag of 15 minutes. The horizontal x-axis represents time (in minutes) ranging (-4500 to +4500). For cross-correlation analysis here, ionospheric parameter is kept fixed and copies of solar storm indices are shifted (lagged) in all cases. Correlation coefficient at each point of lag is calculated, normalized and plotted in the graph.

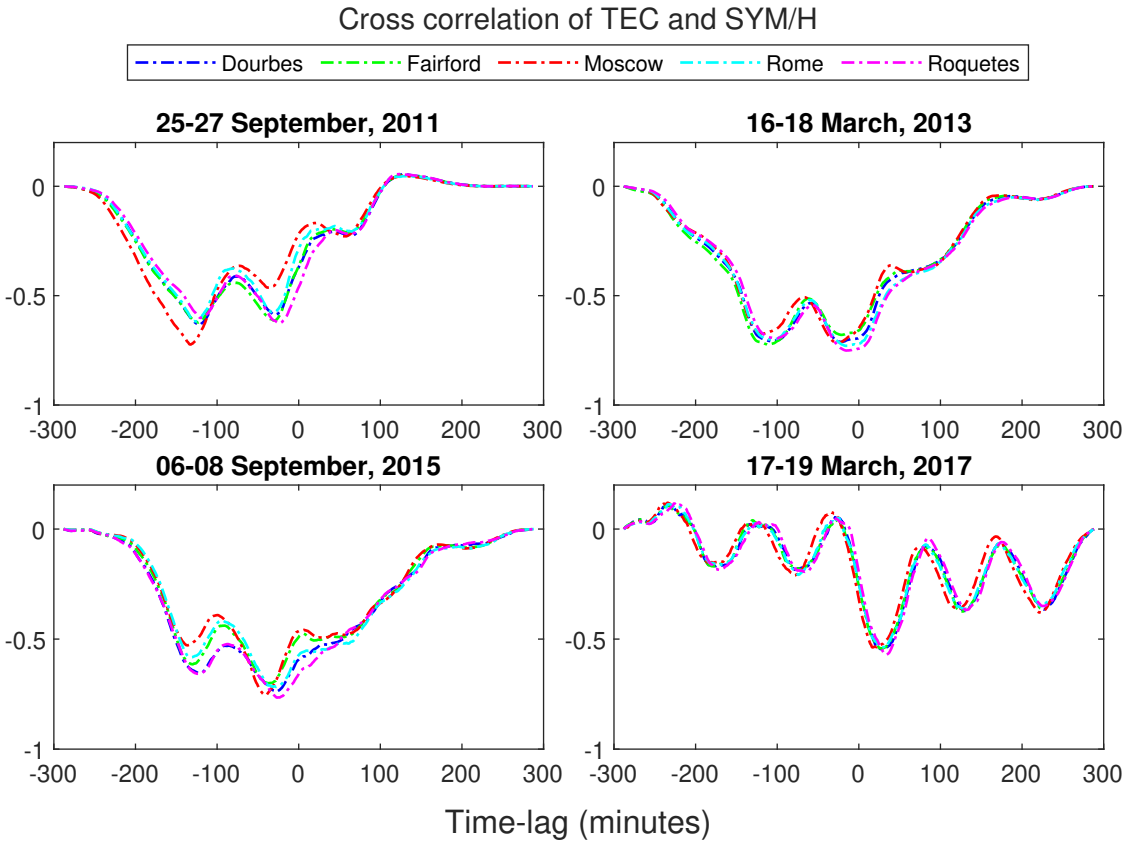

Figure 8. Cross-correlation analysis between TEC and SYM/H during geomagnetic storm of 25–27 September, 2011 (1st Panel), 6–18 March, 2013 (2nd panel), 6–8 September, 2015 (3rd panel) and quiet day on 18-20 March, 2017. X-axis represents time lag (1 unit=15 min) and Y-axis represents correlation coefficient.

In Figure 8, cross-correlation between TEC and SYM/H is analyzed. Here, TEC is kept fixed and copies of SYM/H indices is shifted (lagged). In four of the five stations in the 1st panel, TEC leads SYM/H by 1896 minutes (average) with highest negative correlation of -0.6493. But in Roquetes, max negative correlation of -0.6266 leads by only 345 minutes. Hence, the maximum anti-correlation is not only observed at one point but at two different points. Average maximum negative correlation at these two points are -0.63972 and -0.5734 at time lag of -1878 minutes (1 day 7 hours and 18 minutes) and -450 minutes (7 hours and 30 minutes) respectively.

Similarly, in 2nd panel, in every station except Fairford TEC leads SYM/H by average of 296 minutes with their highest negative correlation of -0.7088 whereas in Fairford it is at 1665 minutes with correlation of -0.7580. Similar to 2011, two minimums can be seen here. The average maximum negative correlation of -0.7174 and -0.7006 occurs at time lag of -300 minutes and -1623 minutes respectively. Here the most negative correlation occurs at -300 minutes (5 hours) time lag but almost equal anti-correlation is observed at -1623 minutes (1 day 3 hours and 3 minutes).

In 3rd panel, each station had their maximum negative correlation around the same time lag. Average correlation of -0.7360 was observed at time lag of -492 minutes (8 hours and 12 minutes). This result matches better with the result of 2nd panel. The quiet day shows moderate anti-correlation with TEC lagging behind SYM/H by about 7 hours in 4th panel.

All three cross correlation analysis of TEC and SYM/H shows high negative correlation between the variables. At least 5 hours of lead in variation of total electron content is observed when compared to the SYM/H index. Almost equal evidence of TEC leading SYM/H by just more than one day can also be obtained from the analysis. This explains the occurrence of positive storm 1 day prior to the sudden storm commencement (SSC). The mechanism of pre-storm phenomenon (positive storm before main phase of the storm in mid-latitude region and negative ionospheric storm phase in the equatorial region) is an unanswered problem in ionospheric physics (Danilov, 2001) and (Chukwuma, 2010).

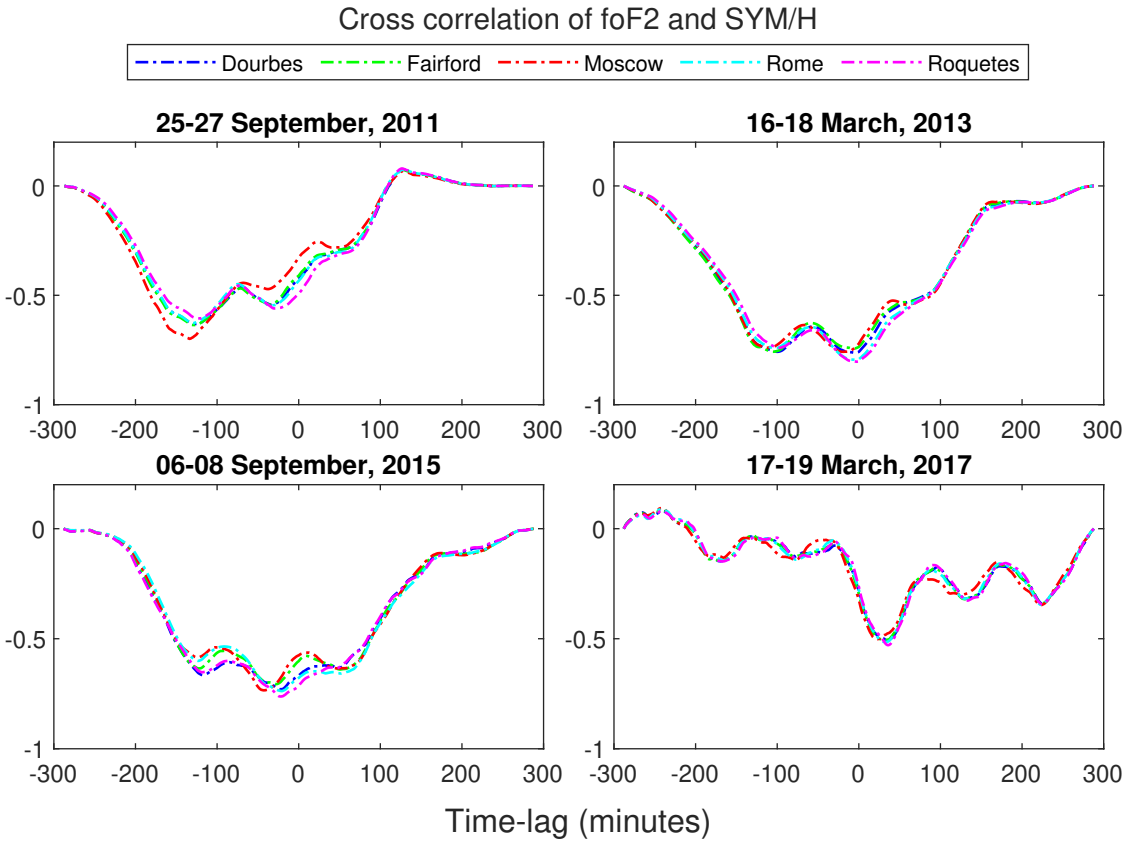

Figure 9. Cross correlation analysis between foF2 and SYM/H during geomagnetic storm of 25–27 September, 2011 (1st Panel), 6–18 March, 2013 (2nd panel), 6–8 September, 2015 (3rd panel) and quiet day on 18-20 March, 2017. X-axis represents time lag (1 unit=15 min) and Y-axis represents correlation coefficient.

In Figure 9, cross-correlation analysis between foF2 and SYM/H is plotted. Here, foF2 is kept fixed and copies of SYM/H indices is shifted for cross-correlation analysis. In two of the five stations in the 1st panel, Durbes and Fairford, foF2 leads SYM/H by 1905 minutes with approximately -0.63 negative correlation while Moscow shows maximum negative correlation of -0.6992 with lag of 2010 minutes. Roquetes and Rome show negative correlation of -0.6054 and -0.6275 respectively with respective time lag of -1815 and -1935 minutes. At average, foF2 leads SYM/H by 1914 minutes(1 day 7 hours 54 minutes) with highest negative correlation of -0.6399.

Similarly, in second pannel, all stations have perfectly overlapped unlike Moscow in 2011. It was found that three of five stations, Durbes, Rome and Roquetes, have minimum time lag of -60 minutes from all panels with maximum negative correlation of -

0.7631 ,-0.7949 and -0.8035 respectively. Moscow also shows a maximum negative correlation of -0.7582 with a minimum time lag of -285 minutes (4 hours and 45 minutes) while Fairford shows minimum negative correlation of -0.7580 but with maximum time lag of -1575 minutes (1 day 2 hours and 15 minutes). In the second panel two minimas with high negative correlation are observed with foF2 leading SYM/H by at least 1 hour to more than a day.

In panel 3, every station has its highest negative correlation coefficient around the same time lag.The average of -0.7342 correlation coefficient at lag of -408 minutes (6 hours 48 minutes) is observed. In panel 4, foF2 lags behind SYM/H by about 7 hours with moderate anti-correlation.

All three cross correlation analysis of FoF2 and SYM/H shows high negative correlation with at least 6 hours of lead in FoF2 signatures compared to the SYM/H index. Also, evidence of FoF2 leading SYM/H with more than one day can also be obtained from the analysis. This analysis matches well with the cross-correlation analysis between TEC and SYM/H. This shows the occurrence of pre-storm phenomena 1 day prior to the sudden storm commencement (SSC) (Chukwuma, 2010).

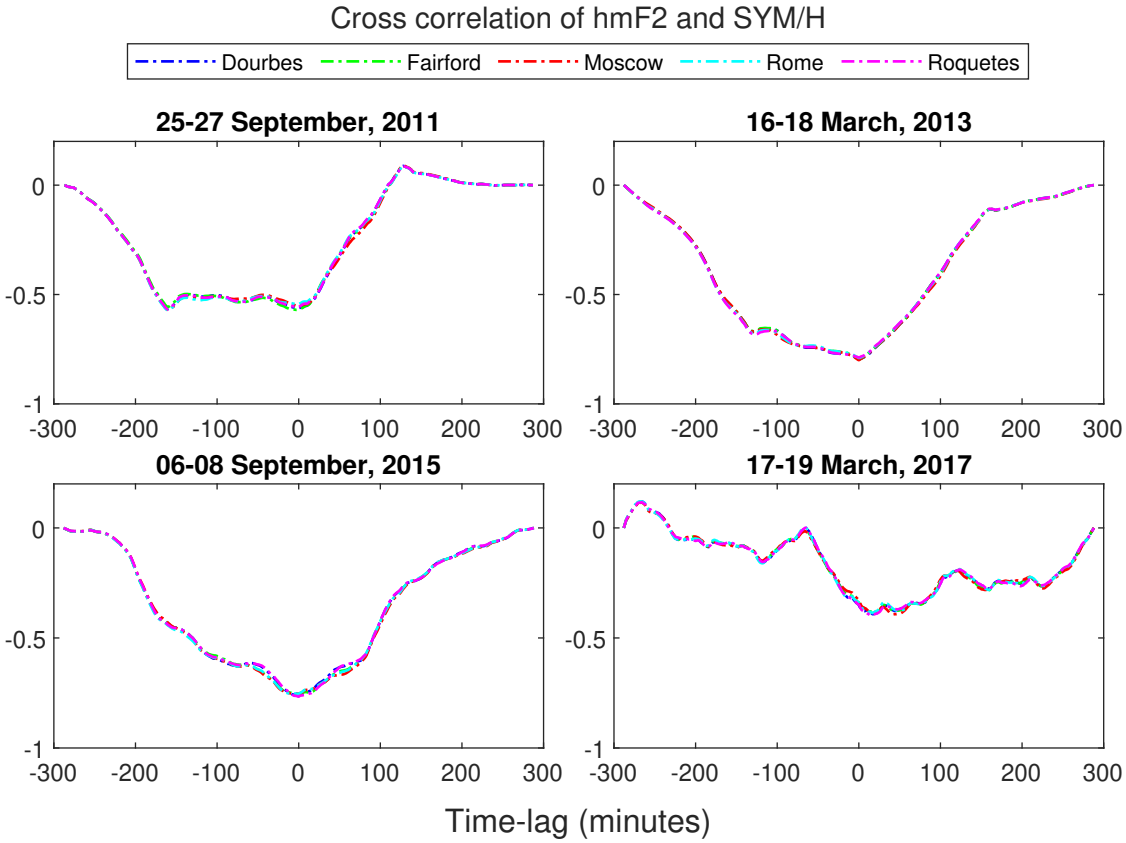

Figure 10. Cross correlation analysis between hmF2 and SYM/H during geomagnetic storm of 25–27 September, 2011 (1st Panel), 6–18 March, 2013 (2nd panel), 6–8 September, 2015 (3rd panel) and quiet day on 18-20 March, 2017. X-axis represents time lag (1 unit=15 min) and Y-axis represents correlation coefficient.

Figure 10 represents cross-correlation between hmF2 and SYM/H index. In this figure hmF2 is kept fixed and copies of SYM/H indices is lagged. In panel 1, there is moderate negative correlation of -0.5703 between the variables at time lag zero but almost equal anticorrelation is seen at time lag of -2400 minutes and throughout the points in

between. In 2nd panel, high negative correlation of -0.7945 is observed at zero lag. Similarly 3rd panel also shows high anticorrelation of -0.7945 with no lag. Compared to other panels, panel 4 has relatively low correlation at zero lag with correlation less than 0.5. So, high anti-correlation between the hmF2 and SYM/H is observed at zero lag.

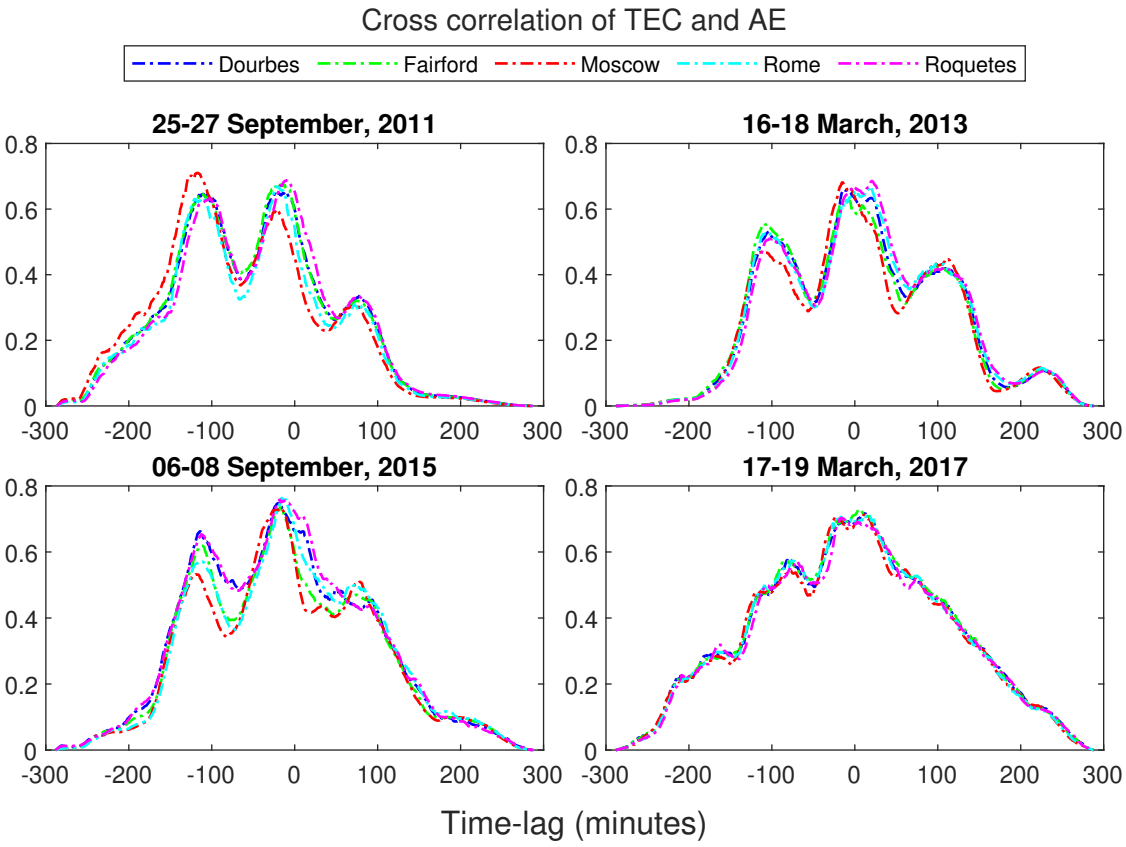

Figure 11. Cross correlation analysis between TEC and AE index during geomagnetic storm of 25–27 September, 2011 (1st Panel), 6–18 March, 2013 (2nd panel), 6–8 September, 2015 (3rd panel) and quiet day on 18-20 March, 2017. X-axis represents time lag (1 unit=15 min) and Y-axis represents correlation coefficient.

Cross-correlation between TEC and AE index is analyzed in Figure 11. In panel 1, two maxima can be observed with TEC leading AE by about 4 hours and more than a day with correlation of 0.7. In the 2nd panel, highest correlation of 0.6649 can be observed at 0 minute time lag.

In the third panel, TEC leads AE by 4 hours with highest correlation of 0.7486. So from the above result it can be said that TEC leads AE by zero to a few hours where there is high correlation between the variables but also moderate correlation between the variables can be observed when TEC led AE index by a day. Here, in 4th panel, high correlation of 0.7 is seen at no lag. This result corresponds well with the result of cross-correlation analysis between TEC-SYM/H, foF2-SYM/H and foF2-AE as two stationary points can be seen in all the graph around same time lag.

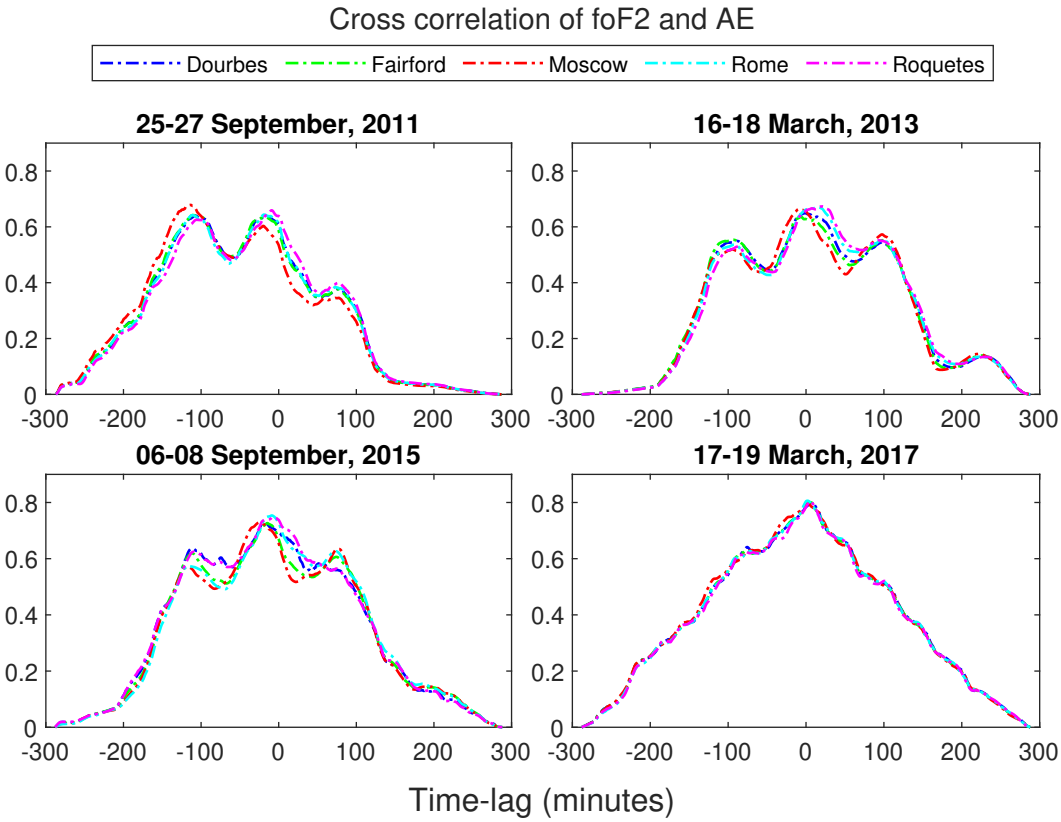

Figure 12. Cross correlation analysis between foF2 and AE index during geomagnetic storm of 25–27 September, 2011 (1st Panel), 6–18 March, 2013 (2nd panel), 6–8 September, 2015 (3rd panel) and quiet day on 18-20 March, 2017. X-axis represents time lag (1 unit=15 min) and Y-axis represents correlation coefficient.

In Figure 12, cross correlation between AE index and foF2 is analyzed. In 3 of the 5 stations, Dourbes, Fairford, Moscow, of 1st panel, foF2 leads AE by 1 day 3 hours 40 minutes (average) with highest positive correlation of 0.6536. While in other 2 stations, Rome and Roquetes, there is the highest positive correlation of 0.6442 and 0.6594 when foF2 leads AE by 4 hours 45 minutes and 2 hours 15 minutes respectively. Similar to all other cross-correlation analysis of TEC and foF2, the red curve (Moscow) in the first panel has higher correlation coefficient in the left stationary point where the ionospheric parameter led solar storm indices by more than 24 hours. This indicates high pre-storm effect in Moscow in the first event as compared to the other events.

Similarly in 2nd panel, in all the stations, foF2 leads AE by 1 hour with highest positive correlation of 0.6582. In 3rd panel, each station had their maximum positive correlation around the same time lag. Average correlation of 0.65 was observed at a time lag of -14.4 (3 hours and 36 minutes). 4th panel shows high correlation at zero time lag. This result corresponds better with the result of 2013. All three cross correlation analysis of foF2 and AE index shows at least 1 hours of lead in variation of foF2 when compared to the AE index with moderate positive correlation.

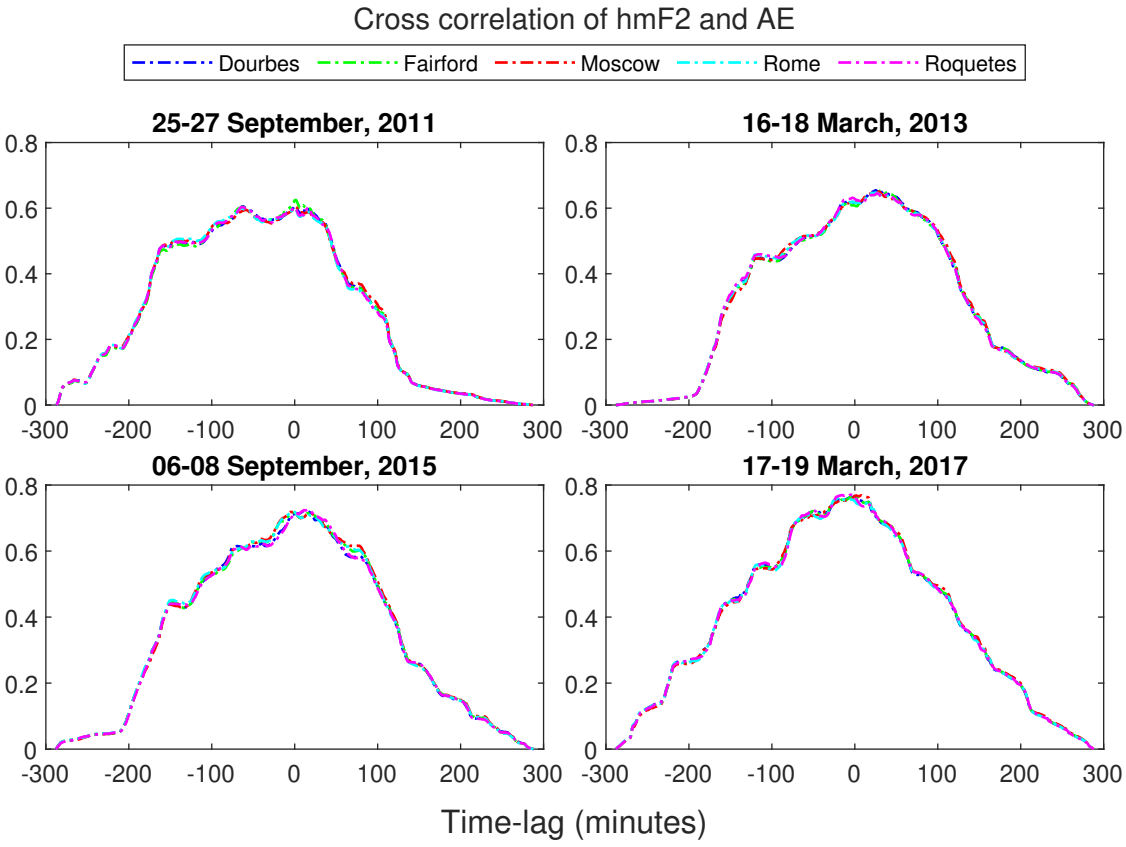

Figure 13. Cross correlation analysis between hmF2 and AE index during geomagnetic storm of 25–27 September, 2011 (1st Panel), 6–18 March, 2013 (2nd panel), 6–8 September, 2015 (3rd panel) and quiet day on 18-20 March, 2017. X-axis represents time lag (1 unit=15 min) and Y-axis represents correlation coefficient.

In Figure 13, cross correlation between hmF2 and AE index is analyzed. In the 1st panel, three stations show highest correlation of 0.6 at time lag of -945 minutes (15 hours and 45 minutes). Fairford shows the highest positive correlation of 0.6246 with time lag of just -15 min which is similar to that of Moscow with correlation of 0.6047 respectively.

But 2nd panel, in all the stations, AE leads hmF2 by average of 411 minutes(6 hours and 51 minutes) with highest positive correlation of 0.6501. In 3rd panel, in all stations, hmF2 lags behind AE by maximum positive correlation of 0.7207 by 72 minutes. There is high correlation in panel 4 at zero lag.

From this result it can be seen that the average lead or lag between hmF2 and AE index is about ±2 hours depending upon the type of storm with moderate positive correlation.

5 Conclusion

In a nutshell, the following conclusions can be drawn out from the cross-correlation analysis of ionospheric parameters and solar storm indices.

1. It is observed that the values of Total Electron Content (TEC) and F2 region critical frequency(foF2) for the events with presence of Sudden Storm Commencement (SSC) had a strong latitudinal dependence in mid-latitude regions with stations at higher latitude having relatively lower values and those at lower latitudes hav-

ing relatively higher values while the event with gradual storm commencement showed no such dependence.

2. It is found that the positive storm started a day before the events and remained so throughout the main phase, then decreased during the recovery phase.
3. The cross-correlation analysis of TEC and foF2 with solar storm indices shows two stationary points at these two time lags with almost equal magnitude of correlation coefficient. This hints strongly to the occurrence of pre-storm phenomenon at least few hours prior to the main phase of the geomagnetic storm.
4. The Maximum Ionization Height of F2 layer (hmF2), showed no pre-storm effect as highest correlation between hmF2 and solar storm indices occurred mostly at zero time lag.
5. It is observed that there is a strong correlation of Symmetric-H and Auroral Electrojet Indices with other ionospheric parameters. This is attributed to the fact that the coupling mechanism between ionosphere and magnetosphere produces extreme electric field disturbances in the middle low latitude regions.
6. The highest correlation between ionospheric parameters is mostly observed for Event 1 a day prior to main phase of geomagnetic storm before. This might be due to the Event 1 being caused by the most intense solar flare (X1.9 flare) among the events selected which resulted in the strongest pre-storm effects.
7. It is observed that despite Events 1 and 3 having the same seasonal condition, the pre-storm phenemenon is completely different. This difference stems from the nature of the two events i.e. Event 1 occurring with sudden storm commencement and Event 3 without SSC. Also, Moscow, which lies at the highest latitude, gets affected by pre-storm phenomenon much more significantly in Event 1 when compared to other events.

Acknowledgments

In this work, we have used the Omni Web (`http://omni-web.gsfc.nasa.gov/`) for interplanetary magnetic fields, solar wind parameters and geomagnetic indices. Global Ionosphere Radio Observatory (GIRO) `https://giro.uml.edu/` provided the ionospheric parameters. The stations list was obtained from `https://lgdc.uml.edu/common/DIDBFastStationList`. The Authors would like to thank the support provided.

Authors' contributions

All the authors contributed equally to this work.

References

Adekoya, B., Chukwuma, V., Bakare, N., & David, T. (2012). On the effects of geomagnetic storms and pre storm phenomena on low and middle latitude ionospheric f2. *Astrophysics and Space Science*, *340*(2), 217–235.

Adhikari, B., Dahal, S., Sapkota, N., Baruwal, P., Bhattarai, B., Khanal, K., & Chapagain, N. P. (2018). Field-aligned current and polar cap potential and geomagnetic disturbances: A review of cross-correlation analysis. *Earth and Space Science*, *5*(9), 440–455.

Baker, D., Jaynes, A., Li, X., Henderson, M., Kanekal, S., Reeves, G., ... others (2014). Gradual diffusion and punctuated phase space density enhancements of highly relativistic electrons: Van allen probes observations. *Geophysical Research Letters*, *41*(5), 1351–1358.

Bothmer, V., & Schwenn, R. (1994). Eruptive prominences as sources of magnetic clouds in the solar wind. *Mass Supply and Flows in the Solar Corona*, 215–220.

Buonsanto, M. J. (1999). Ionospheric storms—a review. *Space Science Reviews*, *88*(3), 563–601.

Chukwuma, V. U. (2010). On ionospheric phenomena during pre-storm and main phase of a very intense geomagnetic storm. *Acta Geophysica*, *58*(6), 1164–1192.

Crooker, N., & McAllister, A. (1997). Transients associated with recurrent storms. *Journal of Geophysical Research: Space Physics*, *102*(A7), 14041–14047.

Danilov, A. (2001). F2-region response to geomagnetic disturbances. *Journal of Atmospheric and Solar-Terrestrial Physics*, *63*(5), 441–449.

Du, A., Tsurutani, B., & Sun, W. (2011). Solar wind energy input during prolonged, intense northward interplanetary magnetic fields: A new coupling function. *Journal of Geophysical Research: Space Physics*, *116*(A12).

Fagundes, P. R., Cardoso, F., Fejer, B., Venkatesh, K., Ribeiro, B., & Pillat, V. (2016). Positive and negative gps-tec ionospheric storm effects during the extreme space weather event of march 2015 over the brazilian sector. *Journal of Geophysical Research: Space Physics*, *121*(6), 5613–5625.

Foster, J., Fairfield, D., Ogilvie, K., & Rosenberg, T. (1971). *Relationship of interplanetary parameters and occurrence of magnetospheric substorms.* (Tech. Rep.). Univ. of Maryland, College Park.

Fuller-Rowell, T., Codrescu, M., Moffett, R., & Quegan, S. (1994). Response of the thermosphere and ionosphere to geomagnetic storms. *Journal of Geophysical Research: Space Physics*, *99*(A3), 3893–3914.

GAO, Q., LIU, L.-B., ZHAO, B.-Q., WAN, W.-X., ZHANG, M.-L., & NING, B.-Q. (2008). Statistical study of the storm effects in middle and low latitude ionosphere in the east-asian sector. *Chinese Journal of geophysics*, *51*(3), 435–443.

Gonzalez, W., Joselyn, J.-A., Kamide, Y., Kroehl, H. W., Rostoker, G., Tsurutani, B., & Vasyliunas, V. (1994). What is a geomagnetic storm? *Journal of Geophysical Research: Space Physics*, *99*(A4), 5771–5792.

Gonzalez, W. D., & Tsurutani, B. T. (1987). Criteria of interplanetary parameters causing intense magnetic storms (dst¡- 100 nt). *Planetary and Space Science*, *35*(9), 1101–1109.

Gosling, J. (1993a). Coronal mass ejections: The link between solar and geomagnetic activity. *Physics of Fluids B: Plasma Physics*, *5*(7), 2638–2645.

Gosling, J. (1993b). *The solar flare myth in solar-terrestrial physics* (Tech. Rep.). Los Alamos National Lab., NM (United States).

Hargreaves, J. K. (1992). *The solar-terrestrial environment: an introduction to geospace-the science of the terrestrial upper atmosphere, ionosphere, and magnetosphere*. Cambridge university press.

Kawamura, S., Balan, N., Otsuka, Y., & Fukao, S. (2002). Annual and semiannual variations of the midlatitude ionosphere under low solar activity. *Journal of Geophysical Research: Space Physics*, *107*(A8), SIA–8.

Klimenko, M. V., Klimenko, V. V., Zakharenkova, I. E., Ratovsky, K. G., Korenkova, N. A., Yasyukevich, Y. V., ... Cherniak, I. V. (2017). Similarity and differences in morphology and mechanisms of the fof2 and tec disturbances during the geomagnetic storms on 26–30 september 2011. In *Annales geophysicae* (Vol. 35, pp. 923–938).

Kolawole, M. (2003). *Radar systems, peak detection and tracking*. Elsevier.

Lei, J., Liu, L., Wan, W., & Zhang, S.-R. (2005). Variations of electron density based on long-term incoherent scatter radar and ionosonde measurements over millstone hill. *Radio science*, *40*(2), 1–10.

Liu, J., Chen, Y., & Lin, J. (2003). Statistical investigation of the saturation effect in the ionospheric fof2 versus sunspot, solar radio noise, and solar euv radiation. *Journal of Geophysical Research: Space Physics*, *108*(A2).

Liu, L., Wan, W., Ning, B., Pirog, O., & Kurkin, V. (2006). Solar activity varia-

tions of the ionospheric peak electron density. *Journal of Geophysical Research: Space Physics*, *111*(A8).

Liu, W., Xu, L., Xiong, C., & Xu, J. (2017). The ionospheric storms in the american sector and their longitudinal dependence at the northern middle latitudes. *Advances in Space Research*, *59*(2), 603–613.

Lugaz, N., Farrugia, C. J., Smith, C. W., & Paulson, K. (2015). Shocks inside cmes: A survey of properties from 1997 to 2006. *Journal of Geophysical Research: Space Physics*, *120*(4), 2409–2427.

Luhmann, J. (1997). What do we really know about solar wind coupling? *Advances in Space Research*, *20*(4-5), 907–911.

Marques de Souza, A., Echer, E., Bolzan, M. J. A., & Hajra, R. (2018). Cross-correlation and cross-wavelet analyses of the solar wind imf b z and auroral electrojet index ae coupling during hildcaas. In *Annales geophysicae* (Vol. 36, pp. 205–211).

Mendillo, M. (2006). Storms in the ionosphere: Patterns and processes for total electron content. *Reviews of Geophysics*, *44*(4).

Moen, J., Qiu, X., Carlson, H., Fujii, R., & McCrea, I. (2008). On the diurnal variability in f2-region plasma density above the eiscat svalbard radar. In *Annales geophysicae* (Vol. 26, pp. 2427–2433).

Pandit, D., Chapagain, N. P., Adhikari, B., Nemirovskaya, I. A., Gordeev, V. V., Kovalenko, D., ... others (2021). Analysis of the solar wind imf b z and auroral electrojet index during supersubstorms. *Russian Journal of Earth Sciences*, *21*(5), 1–10.

Prölss, G. (1995). *Ionospheric f-region storms, handbook of atmospheric electrodynamics, vol. 2.* CRC Press/Boca Raton.

Prölss, G., & Očko, M. (2000). Propagation of upper atmospheric storm effects towards lower latitudes. *Advances in Space Research*, *26*(1), 131–135.

Rangarajan, G. (1989). Indices of geomagnetic activity. *Geomatik*, *3*, 323–384.

Richards, P. (2001). Seasonal and solar cycle variations of the ionospheric peak electron density: Comparison of measurement and models (paper 2000ja000365). *JOURNAL OF GEOPHYSICAL RESEARCH-ALL SERIES-*, *106*(7; SECT 1), 12–803.

Sethi, N., & Pandey, V. (2001). Comparative study of electron density from incoherent scatter measurements at arecibo with the iri-95 model during solar maximum. In *Annales geophysicae* (Vol. 18, pp. 1630–1634).

Souza, J., Brum, C., Abdu, M., Batista, I., Asevedo Jr, W., Bailey, G., & Bittencourt, J. (2010). Parameterized regional ionospheric model and a comparison of its results with experimental data and iri representations. *Advances in Space Research*, *46*(8), 1032–1038.

Sugiura, M., Kertz, W., Price, A., & Stone, D. (1964). *P. 1. hourly values of equatorial dst for the igy.* Pergamon Press.

Verkhoglyadova, O., Tsurutani, B., Mannucci, A., Mlynczak, M., Hunt, L., Paxton, L., & Komjathy, A. (2016). Solar wind driving of ionosphere-thermosphere responses in three storms near st. patrick's day in 2012, 2013, and 2015. *Journal of Geophysical Research: Space Physics*, *121*(9), 8900–8923.

Volland, H. (1995). *Handbook of atmospheric electrodynamics* (Vol. 2). CRC Press.

Wanliss, J. A., & Showalter, K. M. (2006). High-resolution global storm index: Dst versus sym-h. *Journal of Geophysical Research: Space Physics*, *111*(A2).

Xiong, C., Lühr, H., Wang, H., & Johnsen, M. G. (2014). Determining the boundaries of the auroral oval from champ field-aligned current signatures–part 1. In *Annales geophysicae* (Vol. 32, pp. 609–622).

Youssef, M., Mahrous, A., Mawad, R., Ghamry, E., Shaltout, M., El-Nawawy, M., & Fahim, A. (2012). The effects of the solar magnetic polarity and the solar wind velocity on bz-component of the interplanetary magnetic field. *Advances in space research*, *49*(7), 1198–1202.

Zhang, M.-L., Liu, C., Wan, W., Liu, L., & Ning, B. (2009). A global model of the ionospheric f2 peak height based on eof analysis. In *Annales geophysicae* (Vol. 27, pp. 3203–3212).

Zhang, S.-R., & Holt, J. (2008). Ionospheric climatology and variability from long-term and multiple incoherent scatter radar observations: Variability. In *Annales geophysicae* (Vol. 26, pp. 1525–1537).

Table 1: Table of Stations.

S.No.	Stations Name	URSI	Latitude	Longitude
1.	DOURBES	DB049	50.10	4.60
2.	FAIRFORD	FF051	51.70	358.50
3.	MOSCOW	MO155	55.47	37.30
4.	ROME	RO041	41.80	12.50
5.	ROQUETES	EB040	40.80	0.50

Figure.

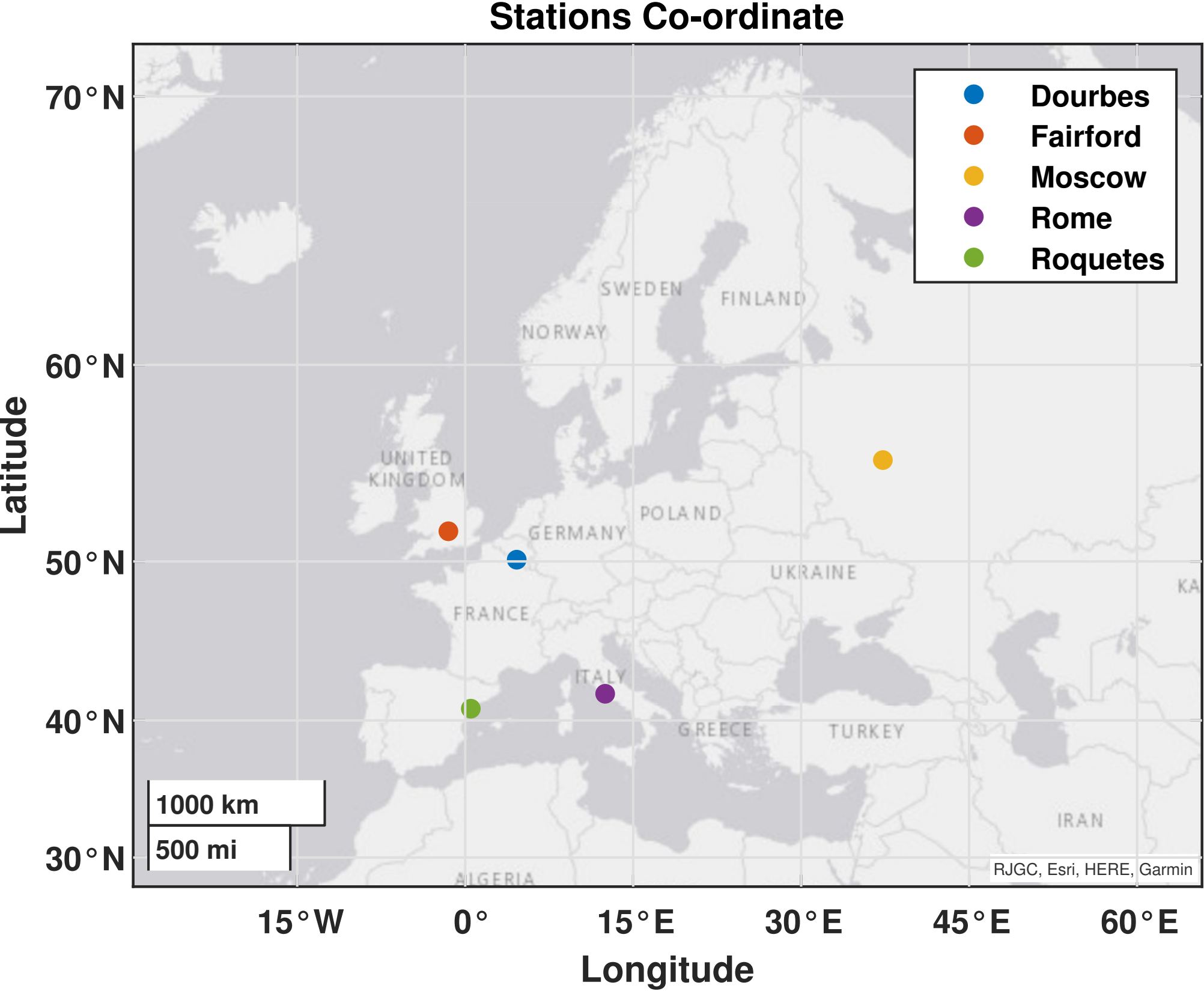
Stations Co-ordinate
Dourbes
Fairford
Moscow
Rome
Roquetes
70°N
60°N
50°N
40°N
30°N
Latitude
15°W
0°
15°E
30°E
45°E
60°E
Longitude
SWEDEN
FINLAND
NORWAY
UNITED KINGDOM
POLAND
GERMANY
UKRAINE
FRANCE
ITALY
GREECE
TURKEY
IRAN
ALGERIA
1000 km
500 mi
RJGC, Esri, HERE, Garmin

Figure.

25-27 September, 2011

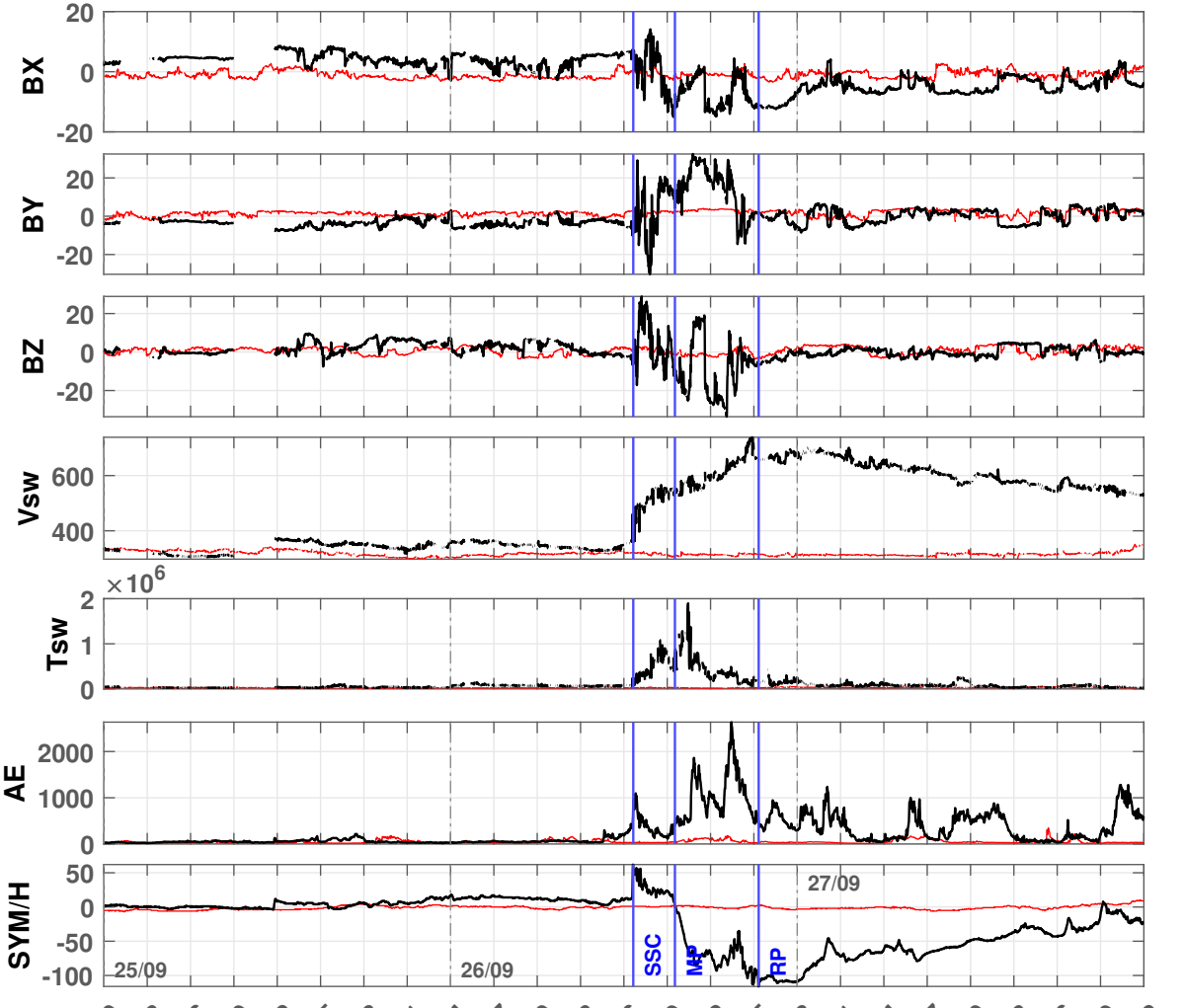

Hours (UTC)

Figure.

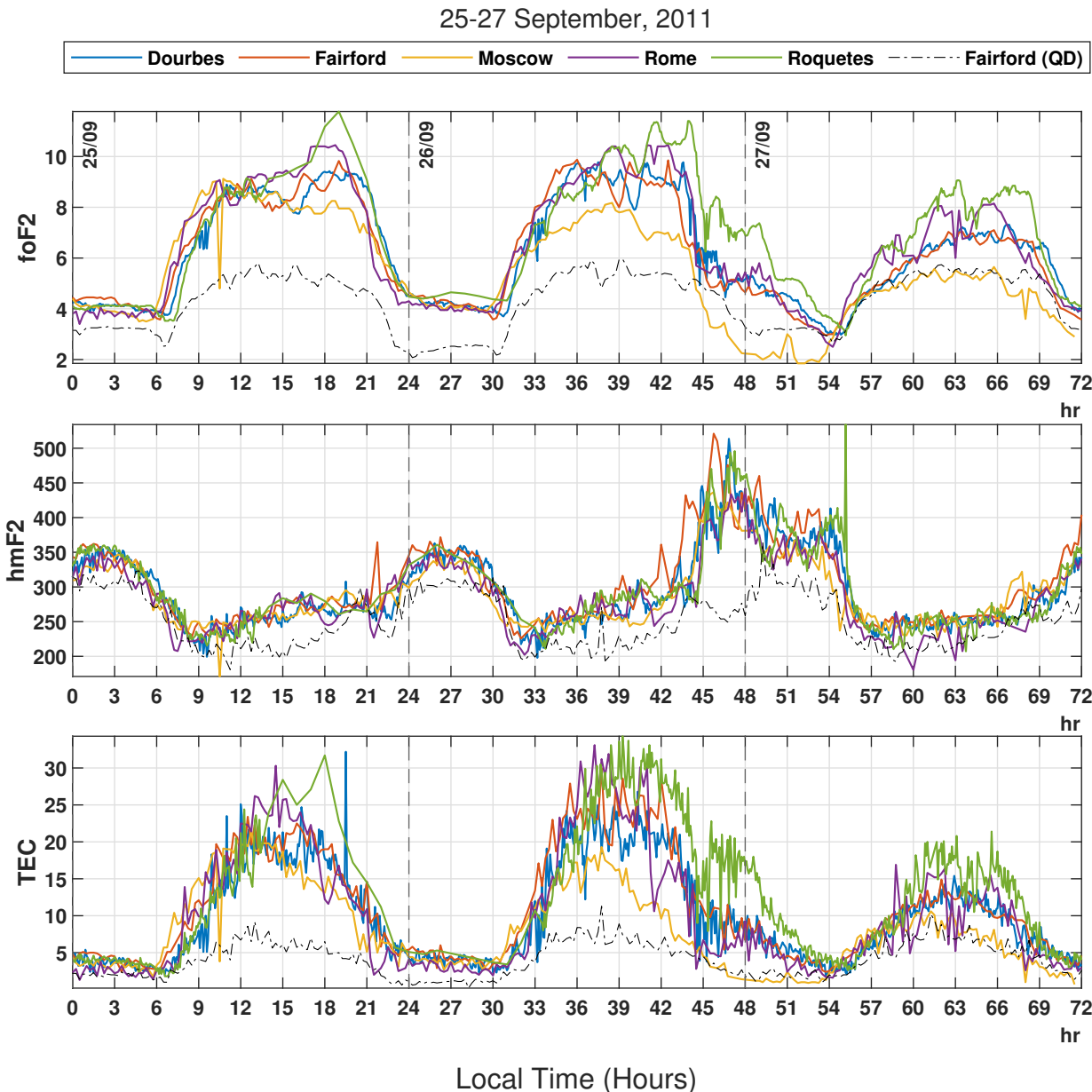
25-27 September, 2011
Dourbes
Fairford
Moscow
Rome
Roquetes
Fairford (QD)
25/09
26/09
27/09
foF2
hmF2
TEC
hr
Local Time (Hours)

Figure.

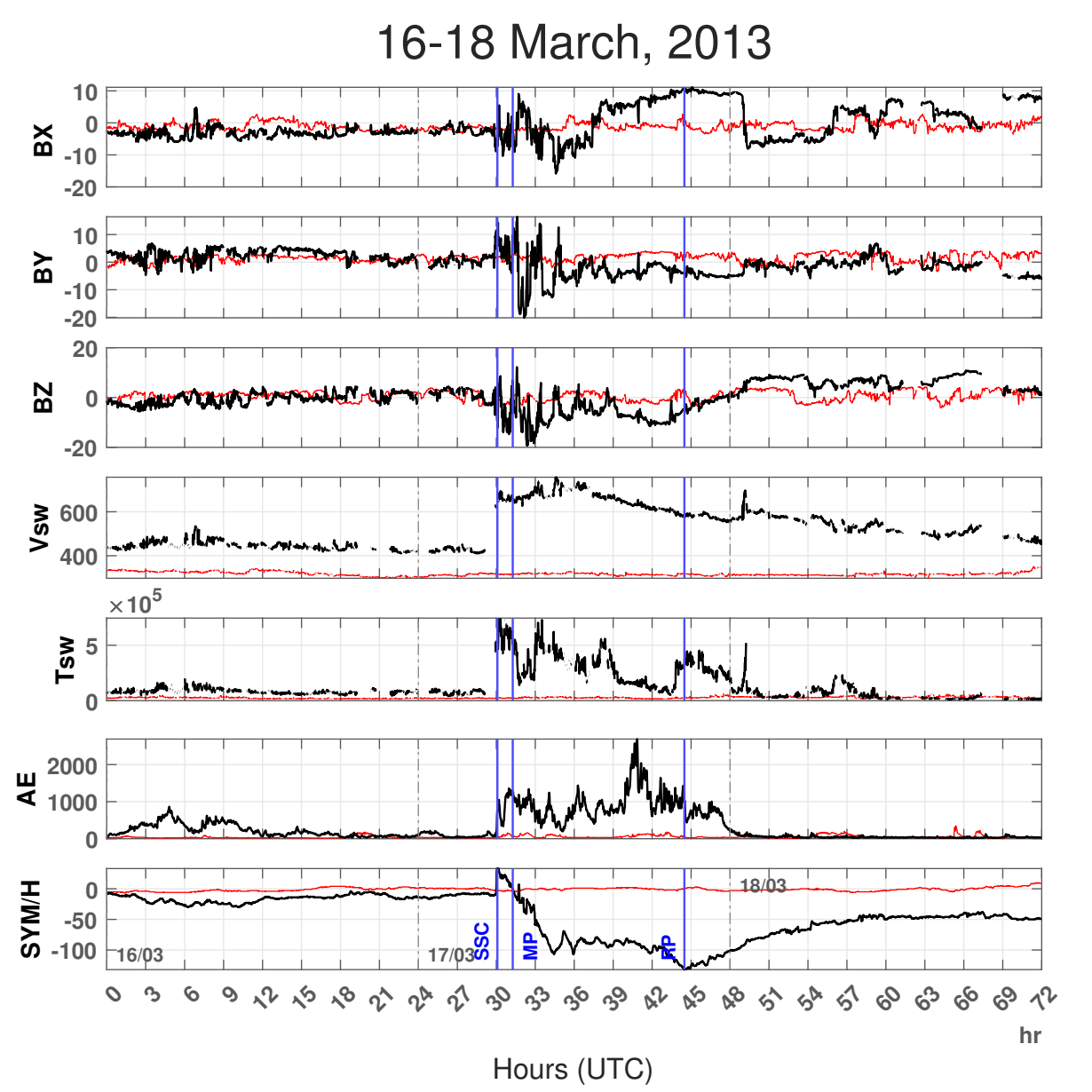
16-18 March, 2013
BX
BY
BZ
Vsw
Tsw
×10^5
AE
SYM/H
16/03
17/03
18/03
SSC
MP
RP
0 3 6 9 12 15 18 21 24 27 30 33 36 39 42 45 48 51 54 57 60 63 66 69 72
hr
Hours (UTC)

Figure.

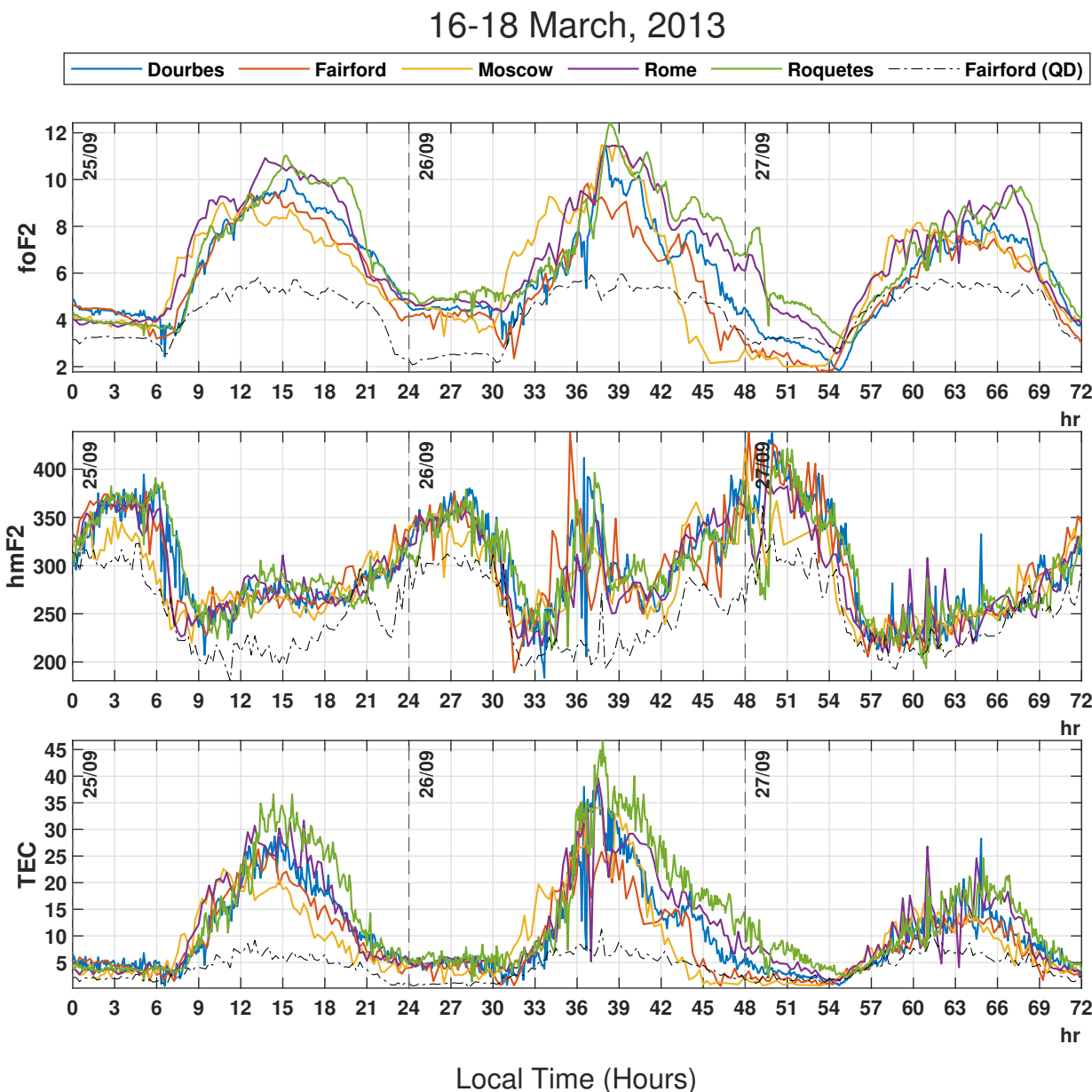
16-18 March, 2013
Dourbes
Fairford
Moscow
Rome
Roquetes
Fairford (QD)
foF2
hmF2
TEC
25/09
26/09
27/09
hr
Local Time (Hours)

Figure.

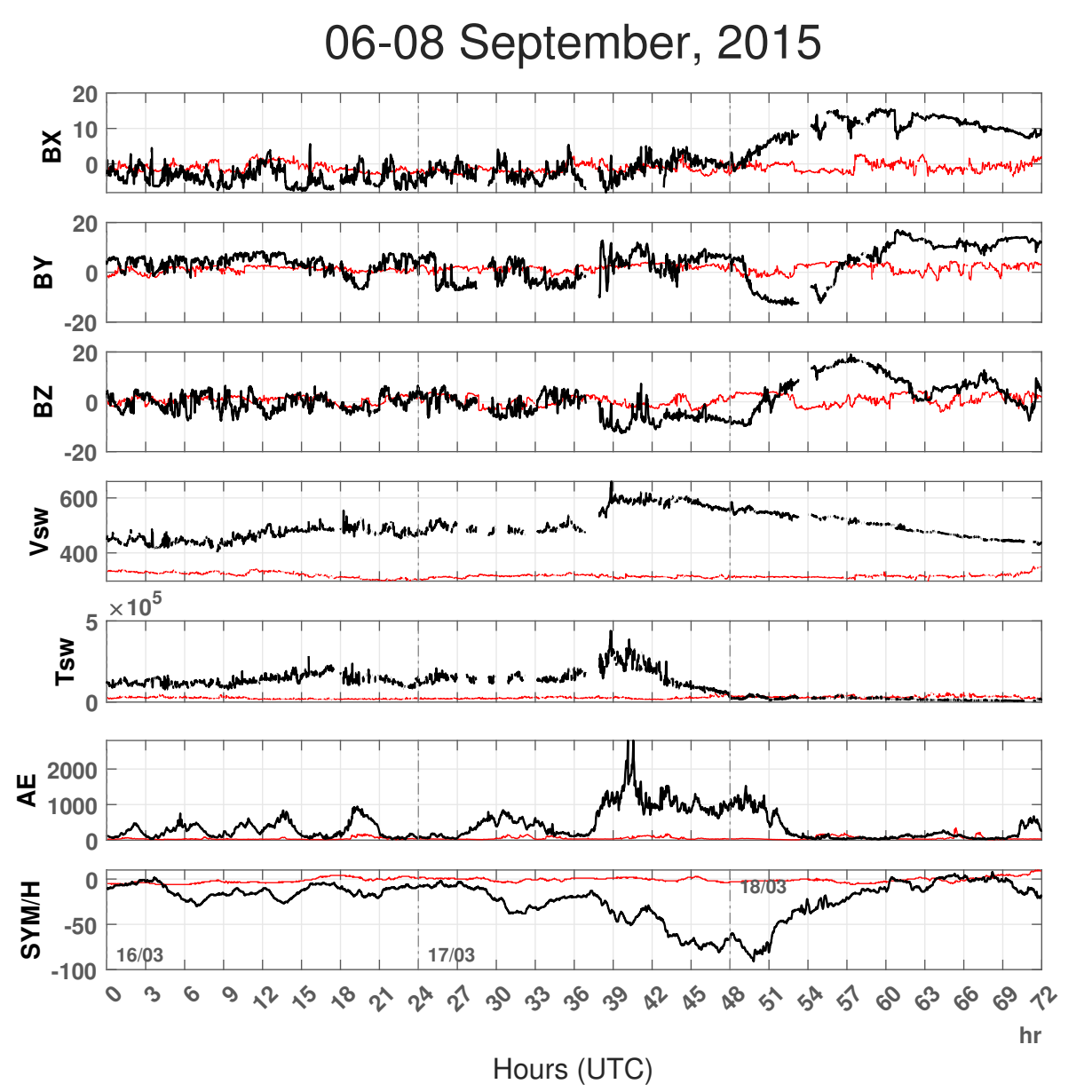
06-08 September, 2015
BX
BY
BZ
Vsw
Tsw
×10^5
AE
SYM/H
16/03
17/03
18/03
0 3 6 9 12 15 18 21 24 27 30 33 36 39 42 45 48 51 54 57 60 63 66 69 72
hr
Hours (UTC)

Figure.

06-08 September, 2015

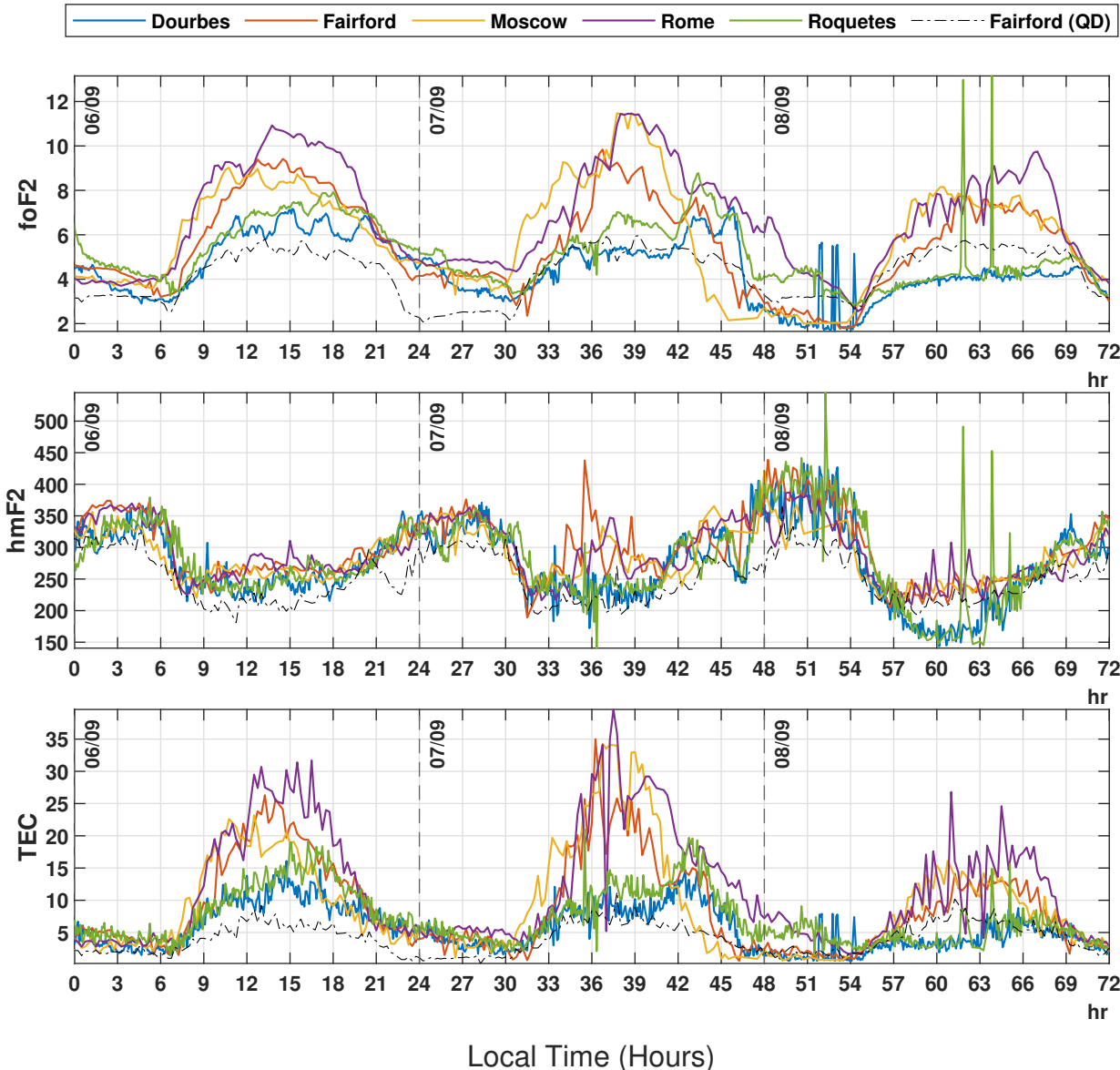

Figure.

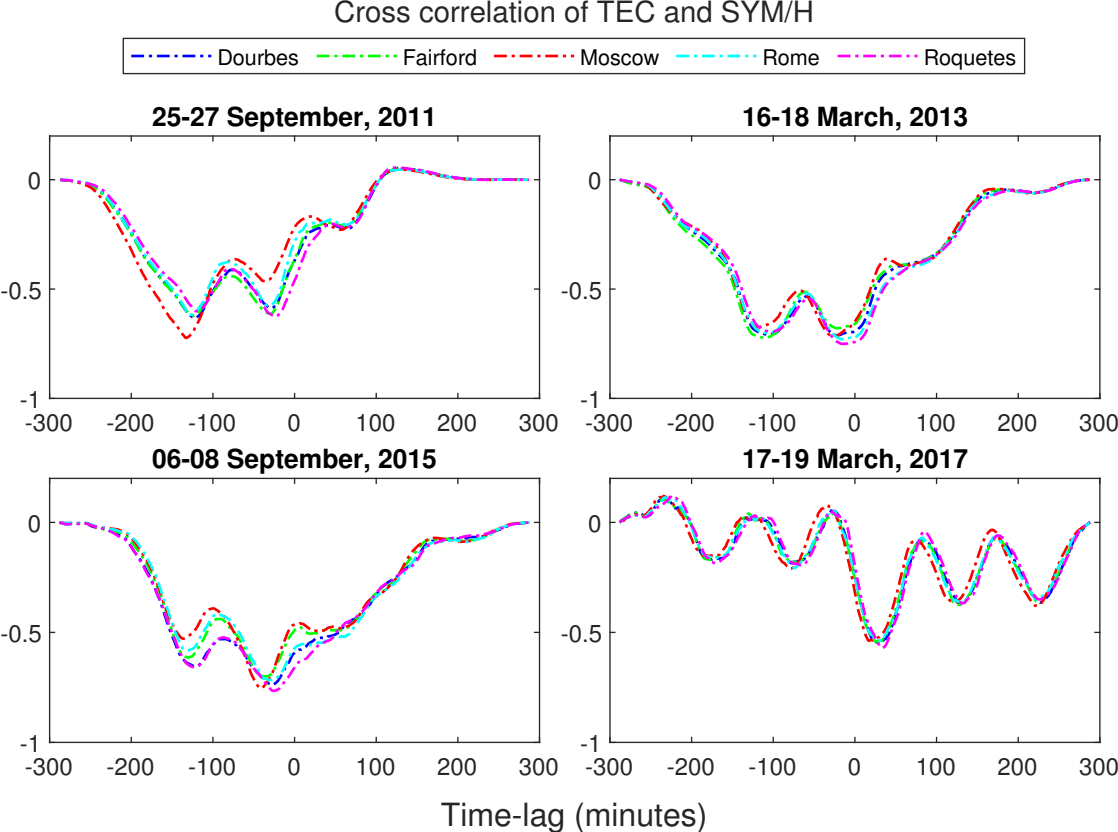
Cross correlation of TEC and SYM/H
Dourbes
Fairford
Moscow
Rome
Roquetes
25-27 September, 2011
16-18 March, 2013
06-08 September, 2015
17-19 March, 2017
0
-0.5
-1
-300
-200
-100
0
100
200
300
Time-lag (minutes)

Figure.

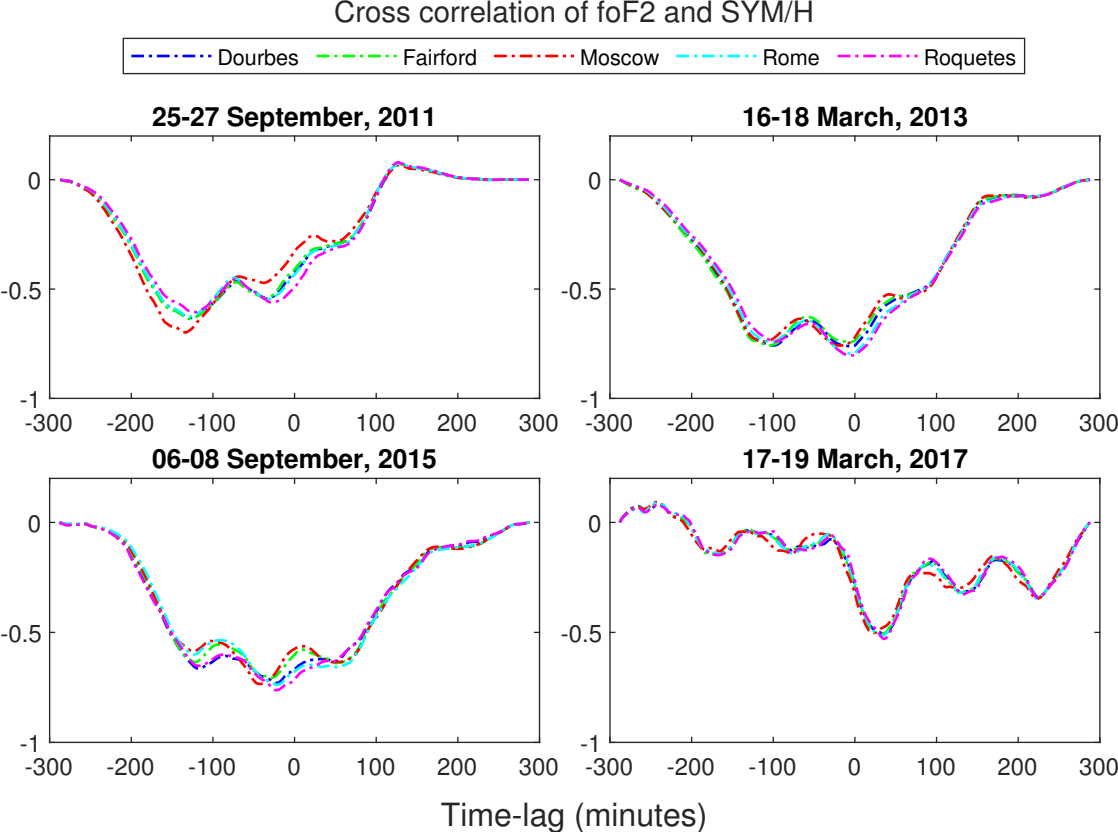
Cross correlation of foF2 and SYM/H
Dourbes
Fairford
Moscow
Rome
Roquetes
25-27 September, 2011
16-18 March, 2013
06-08 September, 2015
17-19 March, 2017
0
-0.5
-1
-300
-200
-100
0
100
200
300
Time-lag (minutes)

Figure.

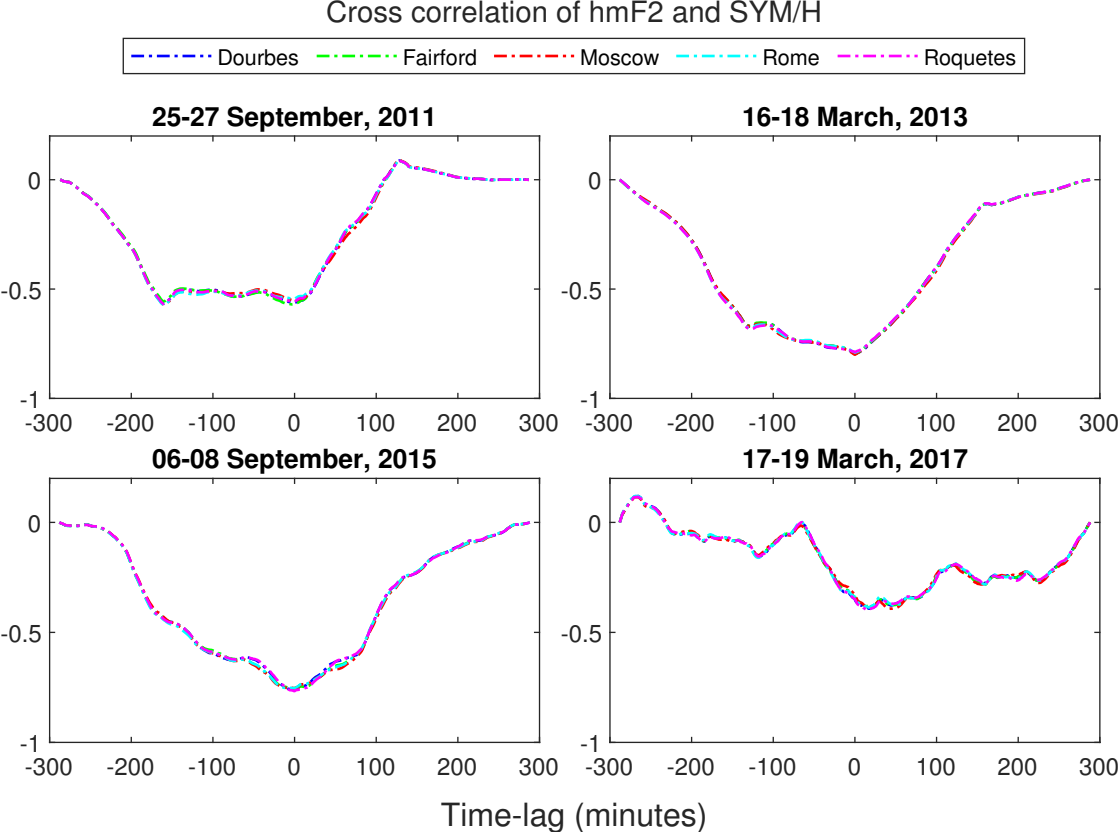
Cross correlation of hmF2 and SYM/H
Dourbes
Fairford
Moscow
Rome
Roquetes
25-27 September, 2011
16-18 March, 2013
06-08 September, 2015
17-19 March, 2017
0
-0.5
-1
-300
-200
-100
0
100
200
300
Time-lag (minutes)

Figure.

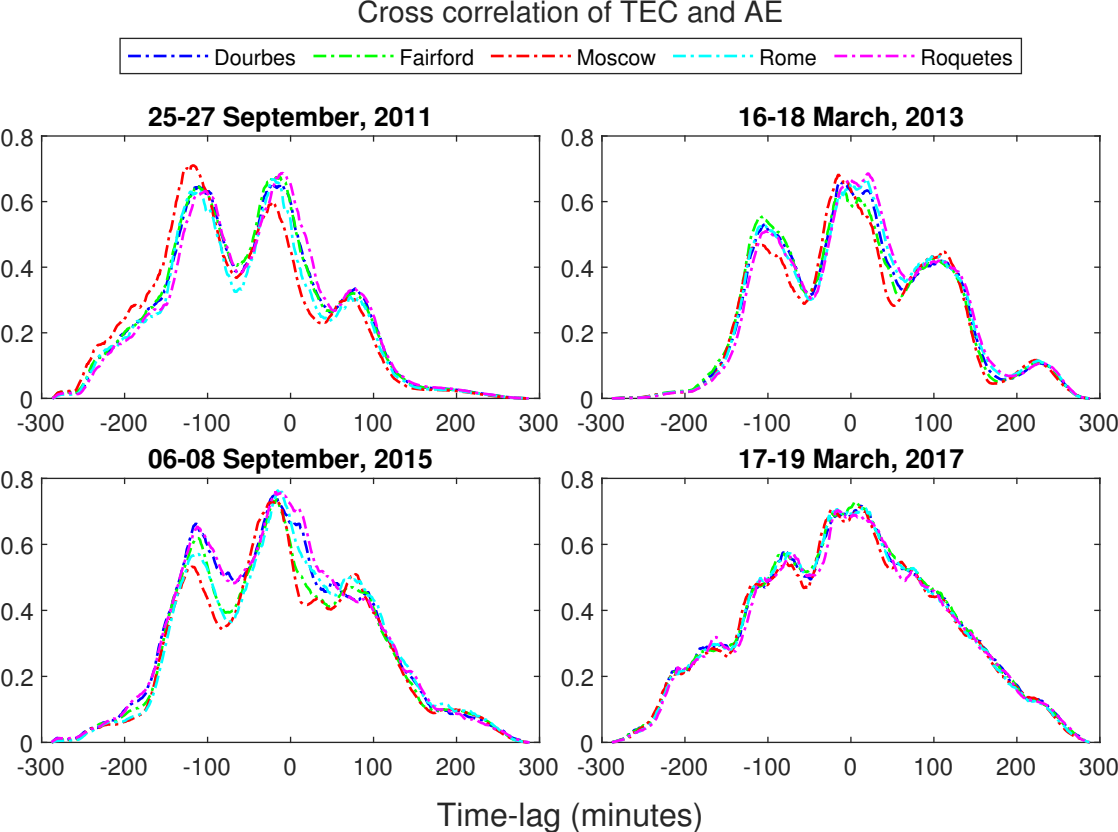
Cross correlation of TEC and AE
Dourbes
Fairford
Moscow
Rome
Roquetes
25-27 September, 2011
16-18 March, 2013
06-08 September, 2015
17-19 March, 2017
0
0.2
0.4
0.6
0.8
-300
-200
-100
0
100
200
300
Time-lag (minutes)

Figure.

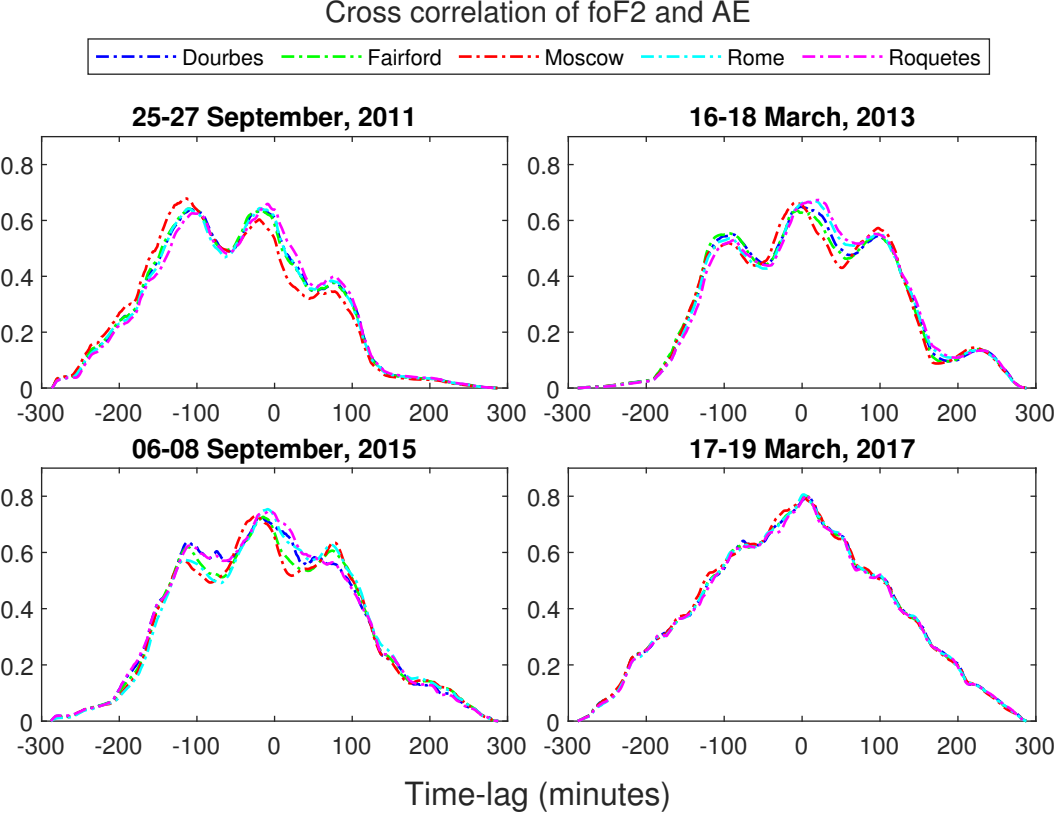
Cross correlation of foF2 and AE
Dourbes
Fairford
Moscow
Rome
Roquetes
25-27 September, 2011
16-18 March, 2013
06-08 September, 2015
17-19 March, 2017
0
0.2
0.4
0.6
0.8
-300
-200
-100
0
100
200
300
Time-lag (minutes)

Figure.

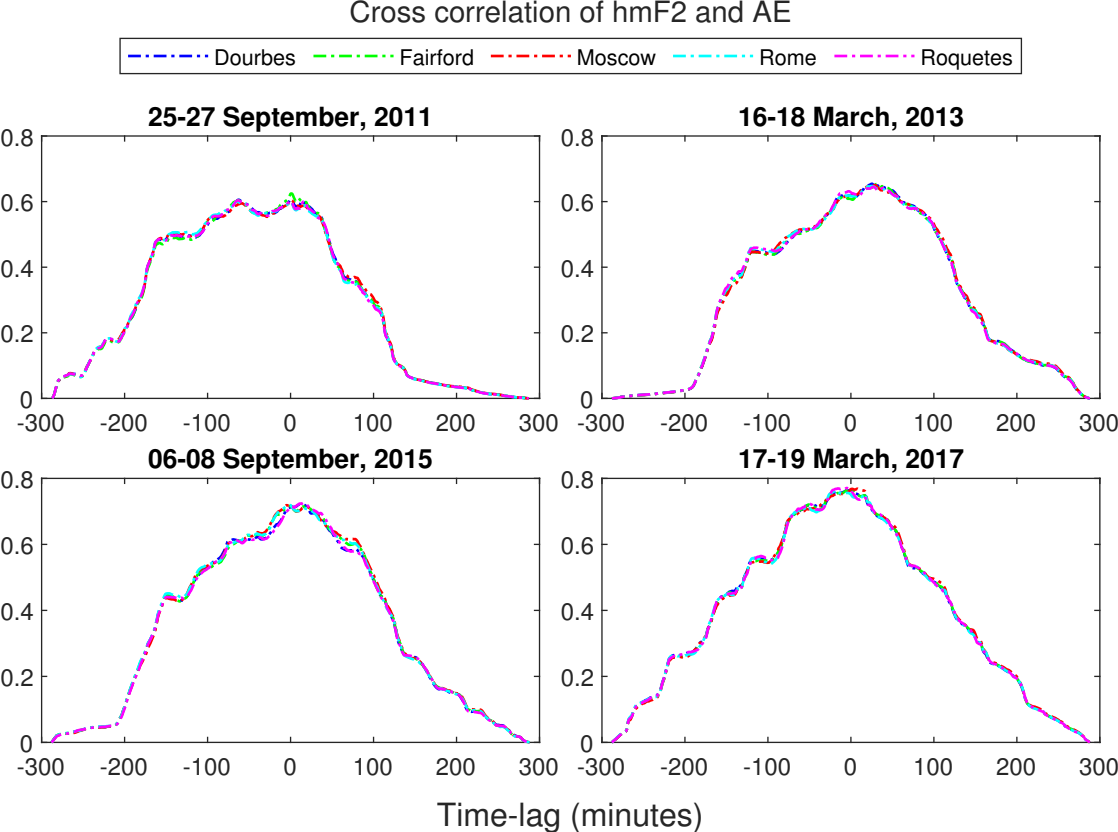
Cross correlation of hmF2 and AE
Dourbes
Fairford
Moscow
Rome
Roquetes
25-27 September, 2011
16-18 March, 2013
06-08 September, 2015
17-19 March, 2017
0
0.2
0.4
0.6
0.8
-300
-200
-100
0
100
200
300
Time-lag (minutes)